Tellus (1994), 46B, 390–418
Printed in Belgium – all rights reserved

TELLUS
ISSN 0280–6509

The Renland ice core. A Northern Hemisphere record of aerosol composition over 120,000 years

By MARGARETA E. HANSSON, *Department of Meteorology, Stockholm University, S-106 91 Stockholm, Sweden* and The Niels Bohr Institute, Department of Geophysics, University of Copenhagen, Haraldsgade 6, DK-2200 Copenhagen, Denmark*

(Manuscript received 8 October 1993; in final form 1 June 1994)

ABSTRACT

The Renland ice core from East Greenland covers a full glacial cycle from the Holocene into the previous Eem interglacial. The first northern hemispheric record of both anions (Cl^-, NO_3^-, SO_4^{2-}, $CH_3SO_3^-$), cations (Na^+, NH_4^+, K^+, Mg^{2+}, Ca^{2+}), total amount of insoluble dust and acidity (measured as solid electrical conductivity) is extracted from this ice core in continuous profiles between 10 and 120 ka B.P. and from the 19th century. The ions measured are in balance during the interglacials but there is a large deficiency of anions during the glacial period. The ice is alkaline during most parts of the glacial period and Ca^{2+} is the totally dominating ion therefore the deficiency of anions is probably due to carbonates (not measured). The concentration of most impurities is higher during glacial stages than the interglacials. The largest increase is found for crustally derived impurities (up to a factor of 10) while the sea salt elements are only slightly enhanced (less than a factor of 2). The concentration of impurities with a strong biogenic component is generally lower during glacial stages than the interglacials. A simple model tests the effect of changes in the physical conditions of the atmosphere influencing transport and deposition processes while keeping the source area and production rate constant. The model results show that the increased glacial concentrations observed for some impurities can be explained entirely by changes in transport and deposition, while the decrease in others may indicate a change in source emissions. The total content of impurities in the glacial atmosphere is higher if physical changes in the atmosphere rather than source emission changes are responsible for the variations observed in the Renland ice core. Thus, physical changes in the atmosphere can have a large impact on the radiative properties of the atmosphere and a climate forcing mechanism may be found in the dynamics of the atmosphere. However, a better understanding of the hydrological cycle and the general circulation of the atmosphere during glacial conditions has to be attained to be able to interpret influences on the global climate of a changed composition of the atmosphere from ice core data.

1. Introduction

The unique information about past climate and atmospheric conditions stored in the polar ice sheets and ice caps has encouraged a large effort in recovering ice cores from various locations. Numerous ice cores add to the picture of geographical differences. A few of these ice cores cover the large climatic changes between glacial and interglacial periods. Ice cores spanning 100,000 years or more have been drilled through the Greenland ice sheet at Camp Century (Hansen and Langway, 1966), Dye 3 (Dansgaard et al., 1982) and lately at Summit (Dansgaard et al., 1993; Grootes et al., 1993) (Fig. 1). The third Greenland surface-to-bedrock ice core was drilled on the small separate Renland ice cap (Fig. 1) in Scoresbysund Fjord, East Greenland in 1988 (Johnsen et al., 1992a). In spite of the short length of 324 m, the Renland ice core covers a full glacial cycle from Holocene into the previous Eem inter-

* Address for correspondence.

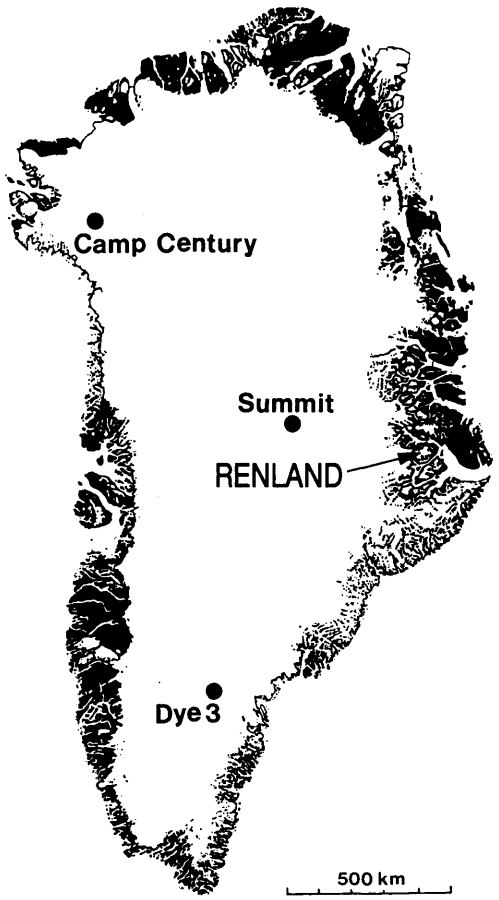

Fig. 1. Map of Greenland showing the drill site of the Renland ice core (71° N, 27° W) and the drill sites of the previous (Camp Century; 77° N, 61° W and Dye 3; 65° N, 44° W) and the latest (Summit; 73° N, 38° W) Greenland deep ice cores.

glacial. The records of atmospheric aerosol composition can be interpreted back to 120 ka B.P.

As the first ice core from the Northern Hemisphere (NH), the Renland ice core was analysed by ion chromatography for both anions (Cl^-, NO_3^-, SO_4^{2-}, $CH_3SO_3^-$) and cations (Na^+, NH_4^+, K^+, Mg^{2+}, Ca^{2+}) in the same samples, together with the total amount of insoluble dust, in time series spanning both interglacial and glacial conditions. The records between 10 and 120 ka B.P. are the first continuous ion records ever obtained for this period. An acidity record is obtained from a continuos profile of solid electrical conductivity (ECM). Similar comprehensive studies of both anions and cations, and covering both glacial and interglacial conditions, have previously been performed on ice cores from Antarctica (Palais and Legrand, 1985; Legrand and Delmas, 1987a; Legrand et al., 1988). The past climate and atmospheric conditions in Antarctica or the conditions in the Southern Hemisphere (SH) have been revealed. However, extrapolating this information to a global scale is speculative. Depending on the residence time in the atmosphere for the different impurities, the Renland ice core may reflect local conditions on the Greenland east coast, conditions in the North Atlantic region or the conditions in the NH. Some impurities, like the tracers of huge, explosive volcanic eruptions, are seen on a global scale and thus found in ice cores from both hemispheres.

The purpose of this paper is focused on presentation of the new data from the NH and interpretation of the chemical profiles in terms of influence of atmospheric transport and deposition processes on the variations in the extracted ice core records over the last climatic cycle. Many authors have previously attributed the observed increases of impurity concentrations in ice cores during glacial stages to expanded source areas and increased production rates however this hypothesis has not been verified. General circulation models fail to reproduce expanded source areas and increased production rates for dust that could account for the observed concentration changes in ice cores (Joussaume, 1993). The high resolution of the latest data from the Summit ice cores (Fuhrer et al., 1993; Mayewski et al., 1993) has revealed large variations of the impurity content on short time scales (i.e., a few years) which is a further indication that atmospheric changes rather than changes on the earth surface (e.g., variations of sea level and vegetation cover) are the primary reasons for the observed variations.

2. Sampling

The 324.35 m long surface-to-bedrock ice core was recovered from the summit of the Renland ice cap, East Greenland, during a joint Danish-Icelan-

Table 1. *Greenland deep ice cores*

Location and year of recovery	Length (m)	Position	Elevation (m a.s.l.)	Mean annual temperature (°C)	Mean annual accumulation (cm ice eq.)	Distance from coast[a] (km)
Camp Century 1966	1390	77°11′N 61°07′W	1890	−24	38	200(W)
Dye 3 1981	2038	65°11′N 43°50′W	2490	−20	56	150(E)
Renland 1988	324	71°18′N 26°43′W	2340	−18	50	150(E)
Summit GRIP 1992	3029	72°34′N 37°37′W	3240	−32	23	550(E)
Summit GISP2 1993	3053	72°35′N 38°29′W	3208	−31	24	580(E)

[a] Distance from the west coast (W) and east coast (E) of Greenland, respectively.

dic-Swedish project. This relatively thin ice cap allowed dry hole drilling with a shallow drill (Johnsen et al., 1980), thus avoiding contamination by a drilling fluid. The characteristics of the Renland ice core drill site are presented in Table 1, together with the previous and the latest Greenland deep ice core drill sites. The high altitude (2340 m a.s.l.) of the Renland drill site is well above the marine boundary layer which minimises the local marine influence.

The ice core was transported to Copenhagen and all sample preparation was performed in a cold room at −14°C. Samples of a 2.5 cm resolution were cut from along the entire ice core for stable isotope analysis. A continuous acidity profile was established and visible stratigraphy recorded. The samples for ion and dust analyses were cut into 5 cm samples after the outer surfaces exposed to contaminants had been removed, all performed with a stainless-steel microtome knife under clean-room (class 100) conditions. The samples were cut as follows: 55 continuous samples were cut between 86.35 and 89.10 m depth representing the time period A.D. 1812–1820 and 374 continuous samples were cut between 305.80 and 324.35 m depth representing approximately 10–145 ka B.P. The samples were stored frozen in 25 ml Accuvettes and melted immediately before the analyses of dust and major ions. The unused, remaining part of each sample was refrozen and later analysed for methanesulphonate ($CH_3SO_3^-$).

3. Analytical methods

The samples were analysed by chemically suppressed ion chromatography. Major anions (Cl^-, NO_3^-, SO_4^{2-}) were determined using AG5A/AS5A5μ columns with an 29 mM $NaHCO_3$ + 23 mM Na_2CO_3 eluent. The samples were injected from a 400 μl loop. Major cations (Na^+, NH_4^+, K^+, Mg^{2+}, Ca^{2+}) were determined using a TCC1 concentrator column and Cationfastsep I/II columns with an 40 mM HCl + 4 mM DAP.HCl eluent, sample volume 2.8 ml. Insufficient separation between the peaks of Na^+ and NH_4^+ when extremely high concentrations of Na^+ were present prevented a quantitative detection of NH_4^+ in a few samples. The analyses of major ions were performed on an integrated Dionex (4000i/2000i) system.

The precision in the analyses (1 sigma) is estimated at better than ±10% on average for all major ions. The quality of the analyses is summarised in Table 2. Blank samples with purified water contained low but significant concentrations of Cl^-, Na^+, NH_4^+ and K^+. Thus, some contamination of these elements in the ice core samples cannot be excluded. However, several ice core samples contained lower concentrations of these ions than the purified water samples, therefore the purified water itself may be the source of these elements. The precision is estimated from succeeding analyses of different vials with identical

Table 2. *Analytical quality of the ion chromatography analyses*

	Blanks with ultra pure water (μeq/l)	Sample range max (μeq/l)	Sample range min (μeq/l)	Possible blank influence in concentration range high (%)	Possible blank influence in concentration range low (%)	Estimate of precision in concentration range high (%)	Estimate of precision in concentration range low (%)
$CH_3SO_3^-$	0	0.07	0.0002	—	—	10	50
Cl^-	0.3	3.4	0.2	9	100	10	50
NO_3^-	0	5.5	0.3	—	—	2	10
SO_4^{2-}	0	6.6	0.3	—	—	2	6
Na^+	0.3	3.0	0.3	10	100	5	20
NH_4^+	0.08	1.5	0.1	5	80	5	5
K^+	0.06	0.6	0.02	10	100	5	10
Mg^{2+}	0	5.3	0.02	—	—	2	20
Ca^{2+}	0	24	0.06	—	—	5	20

standard solutions of a wide concentration range. Reruns of identical, refrozen samples and also some new cut samples from the same depth intervals showed concentrations within 10% for all elements except NH_4^+. The concentration of the new cut samples was within 5% of the previous result while the refrozen samples showed a 35% higher NH_4^+ concentration in the second run. The risk of meltwater contamination by dissolution of ammonia traces present in the atmosphere has previously attracted attention (Legrand and Delmas, 1987b) and the result in this study only confirms the importance of measuring NH_4^+ immediately after the first melting of the samples.

Methanesulphonate was determined on another system. A sample volume of 3.0 ml was used for most samples, but occasionally a smaller volume was used. The samples were loaded by syringe onto a precolumn and separated on AG4/AS4 columns with 5.55 mM NaOH as an eluent. The precision in the $CH_3SO_3^-$ analyses (1 sigma) is estimated at $\pm 30\%$ on average.

Bulk dust concentrations, i.e., the total mass of insoluble particles, were determined by a 90° laser light scattering technique (Hammer, 1977) with an estimated analytical uncertainty at $\pm 25\%$. The continuous acidity (H^+) profile was determined by measuring the solid ice electrical conductivity by dragging brass electrodes along a fresh surface of the ice core (Hammer, 1980, 1983). The current signal (in μA) was transformed into acidity (μeq H^+/l) by a calibration curve relating the two parameters, the latter being derived from pH measurements on melted samples from a variety of other ice cores and corrected for CO_2 induced ions (Hammer, 1980). The uncertainty in this analysis is estimated at $\pm 10\%$.

The stable oxygen isotope analysis was performed by mass spectroscopy. The $\delta^{18}O$ value, expressed in per mille ($^\circ/_{oo}$), describes the relative deviation of oxygen-18 in the precipitation compared to standard mean ocean water (SMOW). The measuring accuracy is better than $0.1^\circ/_{oo}$. The $\delta^{18}O$ values found in the snow pack on the Greenland ice sheet are shown to be closely related to the local mean annual surface temperature (Dansgaard et al., 1973; Johnsen et al., 1989) and ice core profiles of $\delta^{18}O$ can, with some caution (Johnsen et al., 1972), be interpreted in terms of past climate conditions. When averaged over many years, an increase of $0.7^\circ/_{oo}$ of the mean annual $\delta^{18}O$ value corresponds to about a 1°C increase of the mean annual surface temperature. The interpretation of the Renland $\delta^{18}O$ profile is described in detail elsewhere (Johnsen et al., 1992a; Johnsen and Dansgaard, 1992; Johnsen et al., 1992b).

4. Chronology

The Renland $\delta^{18}O$ profile below 300 m depth is shown on a linear depth scale in Fig. 2. The entire record of the glacial period and the previous interglacial is compressed into the deepest 20 m of the Renland ice core. However, comparisons with the $\delta^{18}O$ profiles from Camp Century, Dye 3 and Summit (Johnsen and Dansgaard, 1992; Johnsen

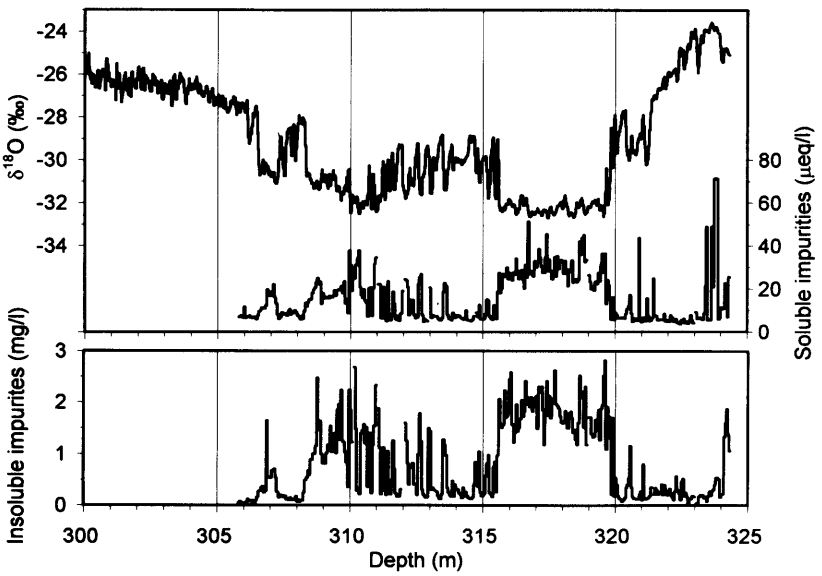

Fig. 2. Top: The Renland $\delta^{18}O$ profile (2.5 cm per sample) for the deepest 25 m on a linear depth scale. Middle: The total amount of analysed soluble impurities. Bottom: The total amount of insoluble impurities (dust).

et al., 1992b) show that the Renland record is well preserved, even in detail, despite the closeness to the bedrock. The only exception is a 4 m thick layer in the Renland ice core, from 5 to 9 m above the bedrock, which is homogeneous with respect to the $\delta^{18}O$ values. This layer has no counterpart in any other ice core or other climatic record. The thickness of this layer that could represent a very long time period with very stable climate must therefore be suggested to be due to other processes than year-by-year deposition of snow followed by regular and undisturbed deformation of the annual layers. The layer has very high concentrations of both soluble and insoluble impurities (Fig. 2) which probably affect the viscosity of the ice. The exaggerated thickness of this layer is therefore suggested to be due to the Boudinage effect (Staffelbach et al., 1988) that causes strongly varying thickness of particular soft layers exposed to long lasting local stresses around discrete obstacles on the bedrock. The more rigid ice closer to the bedrock is apparently unaffected since the $\delta^{18}O$ profile is in accordance with other records.

The Renland ice core was dated by ice flow model calculations (Johnsen and Dansgaard, 1992) with three time scale fix points at distinct events as the end of Younger Dryas 10,720 years B.P., the onset of Bölling 14,000 years B.P. and the culmination of Eem 130,000 years B.P. The entire Boudinage layer, except 15 cm of it, was removed from the record and the remaining parts of the glacial record were compensated for the additional thinning. The time scale beyond the fix point at 130 ka B.P. is highly uncertain. This period, which is the bottom most 55 cm of the ice core, consists of transparent, entirely bubble free ice most probably formed by extensive surface melting since the bedrock temperature ($-13°C$) is far below the pressure melting point. Two shorter periods (i.e., layers of 9 and 21 cm thickness, respectively) between 120 and 130 ka B.P. show similar signs of melting. The $\delta^{18}O$ values in the periods with bubble free ice do not deviate from the $\delta^{18}O$ values in adjacent periods.

The entire $\delta^{18}O$ profile on the calculated time scale is shown in Fig. 3. The conventional marine oxygen isotope stages are indicated. The thinning of annual layers is maximal in the oldest glacial ice which is softer than the underlying Eem interglacial ice. This causes the irregular distribution of the samples on the time scale and the low resolution between 65 and 110 ka B.P. (approx. 1250 years

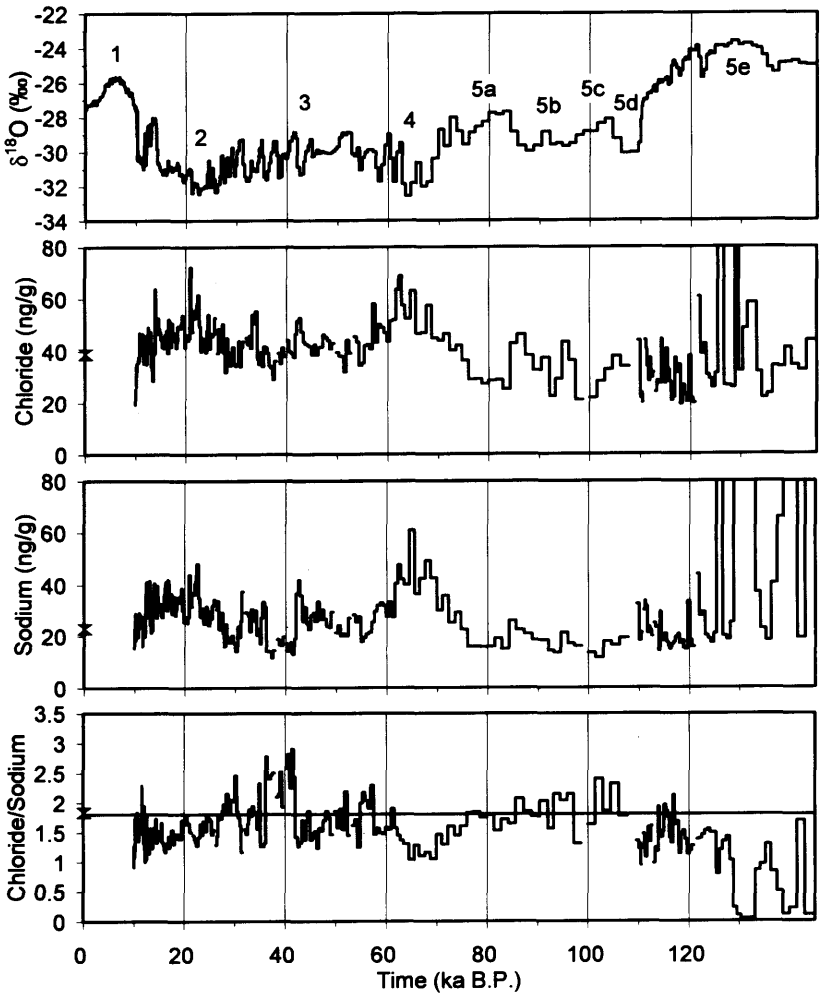

Fig. 3. The Renland $\delta^{18}O$ profile (5 cm per sample) on a calculated time scale. The conventional marine oxygen isotope stages are indicated. Below are the records of Cl^- and Na^+. The weight ratio Cl^-/Na^+ profile is shown at the bottom with the sea water Cl^-/Na^+ ratio (1.8 by weight) indicated. The records are affected by melt layers beyond 122 ka B.P. The mean value of five full years in the late Holocene (A.D. 1813–1815 and 1818–1819) is indicated by a cross to the left in each figure.

per 5 cm sample, cp. 125 and 300 years per 5 cm sample in the periods 10–20 and 110–120 ka B.P., respectively).

5. Results

5.1. The 10–145 ka B.P. profiles

The impurity concentration profiles (shown in Figs. 3, 4 and 5) are divided into three groups according to their variation with climate, i.e., correlation with the $\delta^{18}O$ profile. Anomalous high concentrations of Cl^- (200–500 ng/g), Na^+ (400–1300 ng/g), K^+ (100–400 ng/g) and NO_3^- (250–500 ng/g) are found beyond 122 ka B.P. No anomalies are found in the other ion profiles, although the concentrations of most ions are higher during the culmination of Eem compared to the termination. The samples with anomalous high concentrations are stratigraphically coincident

with the melt layers and post-depositional processes have most probably affected this part of the record. Accordingly, the parts of the records beyond 122 ka B.P. are excluded from all interpretations concerning atmospheric composition. The mean value of five full years in the late Holocene (A.D. 1813–1815 and 1818–1819) is indicated by a cross to the left in each figure for comparison. These mean values may be representative of climate conditions similar to present but without any anthropogenic influence on the impurity concentrations.

The first group contains the typical sea salt elements Cl^- and Na^+ (Fig. 3). The general trend (i.e., variations on the order of tens of thousands of year) of these ions is anti-correlated to the $\delta^{18}O$ profile with enhanced concentrations in periods with colder climate. Also short cold events of hundreds of years are generally accompanied by enhanced concentrations. The ratio between Cl^- and Na^+ in the late Holocene period is identical to the bulk sea water ratio (1.8 by weight). However, an excess of Na^+ (relative to the sea water ratio) is present mainly in stage 2 and 4 in the glacial period. A few samples contain excess Cl^- but the amount is not significant compared to the combined analytical error in the Cl^-/Na^+ ratio. The excess Na^+ may represent an additional source of Na^+ or be due to a fractionation process in the atmosphere where the chloride is lost as gaseous HCl and not deposited together with the sodium. The correlation of excess Na^+ with the crustally derived impurities (cp. Figs. 3, 4) and previous reported excess Na^+ of terrestrial origin (Legrand, 1987) support the hypothesis of an additional crustal source for Na^+, therefore the concentration of Cl^- is used to calculate the sea salt component of other ions.

The second group contains dust, Ca^{2+}, SO_4^{2-}, Mg^{2+} and K^+ (Fig. 4). The impurities in this group also show a clear relationship to the climate. Short cold events during the glacial period are accompanied by highly enhanced concentrations from the background. The background concentrations are fairly constant along the profiles except in the very coldest stages 2 and 4 where they are enhanced. The amplitude of the variations differ between the records and are largest for dust and Ca^{2+}. The high concentrations of dust in the bottom most samples are most probably due to particles scraped off from the bedrock. Large particles were seen with the naked eye in the bottom section of the ice core already at the first inspection at recovery. This was one of the indications of the closeness to the bedrock which terminated the drilling. The bedrock particles indicate that the bottom most 25 cm (i.e., beyond 138 ka B.P. in Fig. 4) do not represent an undisturbed ice stratigraphy.

The third group contains NO_3^-, NH_4^+ and $CH_3SO_3^-$ (Fig. 5). This group of ions is less homogeneous than the previous groups. The general trend of these ions is correlated to the $\delta^{18}O$ profile with low concentrations in periods with colder climate. However, the lowest concentrations of NO_3^- are found in the warm stage 5e and the highest concentrations of NO_3^- and NH_4^+ are found at the end of the glacial period in the cold Younger Dryas event and in the mild Alleröd–Bölling interstadial. Very high concentrations of NH_4^+ are also found during the mild stages 5a and 5c in the beginning of the glacial period. The variations of $CH_3SO_3^-$ are scattered with large variations between succeeding samples, especially beyond 60 ka B.P. where the time resolution is low. An anti-correlation to the $\delta^{18}O$ profile on the time scale of hundreds of years is sometimes found also in this third group. The profile of the molar ratio R between $CH_3SO_3^-$ and non-sea salt (nss) SO_4^{2-} is included in Fig. 4.

The acidity signal (H^+) in Fig. 4 has to be treated separately since the apparent correlation with the $\delta^{18}O$ profile is caused by the increase of alkaline impurities in the glacial period. It is the strong acids HNO_3 and H_2SO_4 (and sometimes HCl and HF from volcanic eruptions) that contribute to the acidity signal in the interglacial periods. Although the sources of these acids were active during the glacial period, the strong enhancement of alkaline impurities caused a total neutralisation of the acidity signal.

5.2. *Comparison with other Greenland data*

Mean values and standard deviation for each impurity in the different climatic stages are presented in Table 3. The division into climatic stages is based on the conventional marine oxygen isotope stages. The ion concentrations are expressed as microequivalents per litre (μeq/l) and the dust content is expressed as mass fraction (ng/g). The concentration of Cl^- is used to calculate the non-sea salt (nss) component of other ions, $\{X\}_{nss} =$

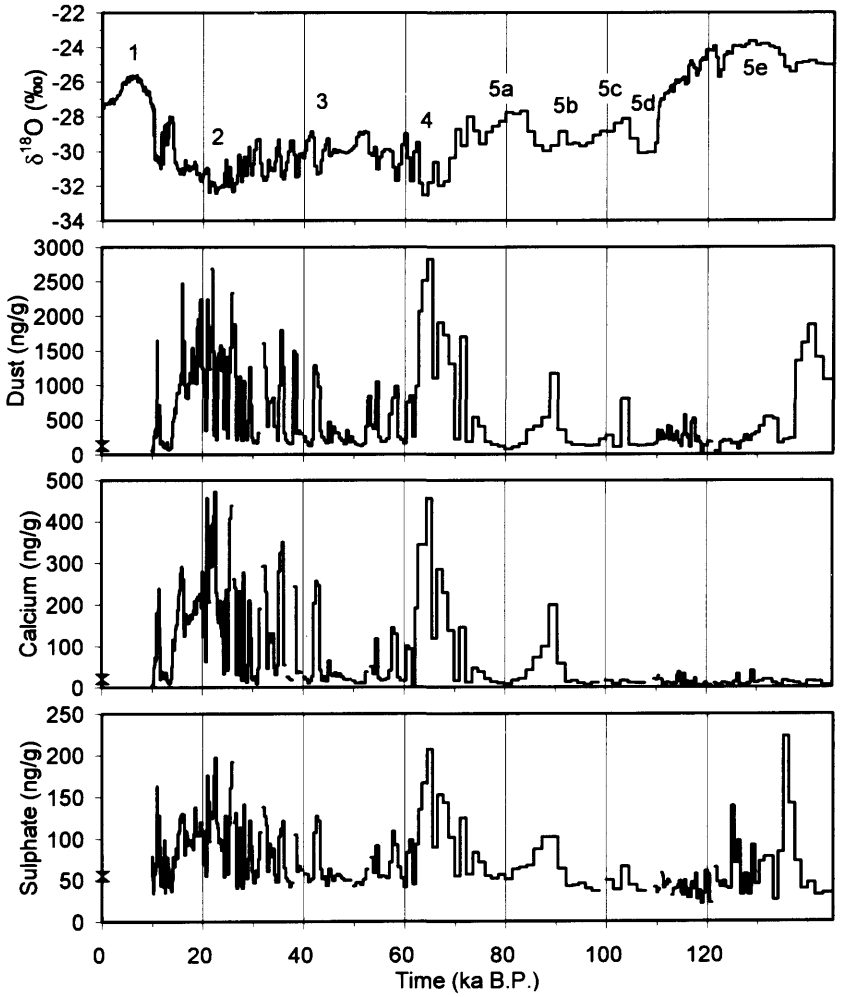

Fig. 4. The Renland ice core profiles of $\delta^{18}O$, dust, Ca^{2+}, SO_4^{2-}, Mg^{2+}, K^+, H^+ and the molar ratio R ($CH_3SO_3^-$/nss SO_4^{2-}), respectively. The records are affected by melt layers beyond 122 ka B.P. and therefore is the molar ratio R calculated as $CH_3SO_3^-$/total SO_4^{2-} beyond 122 ka B.P. The mean value of five full years in the late Holocene (A.D. 1813–1815 and 1818–1819) is indicated by a cross to the left in each figure.

$\{X\}_{tot} - \{X\}_{ss}$, assuming a sea water composition corresponding to $\{Ca^{2+}\}_{ss} = 0.038\{Cl^-\}$, $\{SO_4^{2-}\}_{ss} = 0.10\{Cl^-\}$, $\{Mg^{2+}\}_{ss} = 0.19\{Cl^-\}$ and $\{K^+\}_{ss} = 0.019\{Cl^-\}$. Ratios given in Table 3 are mean values of the individual ratios. They deviate sometimes from the ratios of the mean values, especially for the late Holocene period where seasonal differences are found between different samples.

Stage 1 is represented by two time series in the late Holocene and Pre-boreal, respectively. These periods are not representative of the mean climate in stage 1. The post-glacial climatic optimum at around 6 ka B.P. was 2.5°C warmer than present. Thus, only the colder Holocene interglacial climate is represented in this study. The late Holocene concentrations are mean values of five full years in the period A.D. 1813 to 1819. The eruption of the volcano Tambora in A.D. 1815 caused high concentrations of H^+ and SO_4^{2-} in the precipitation of the two years that followed. These two years, A.D. 1816 and 1817, are excluded from

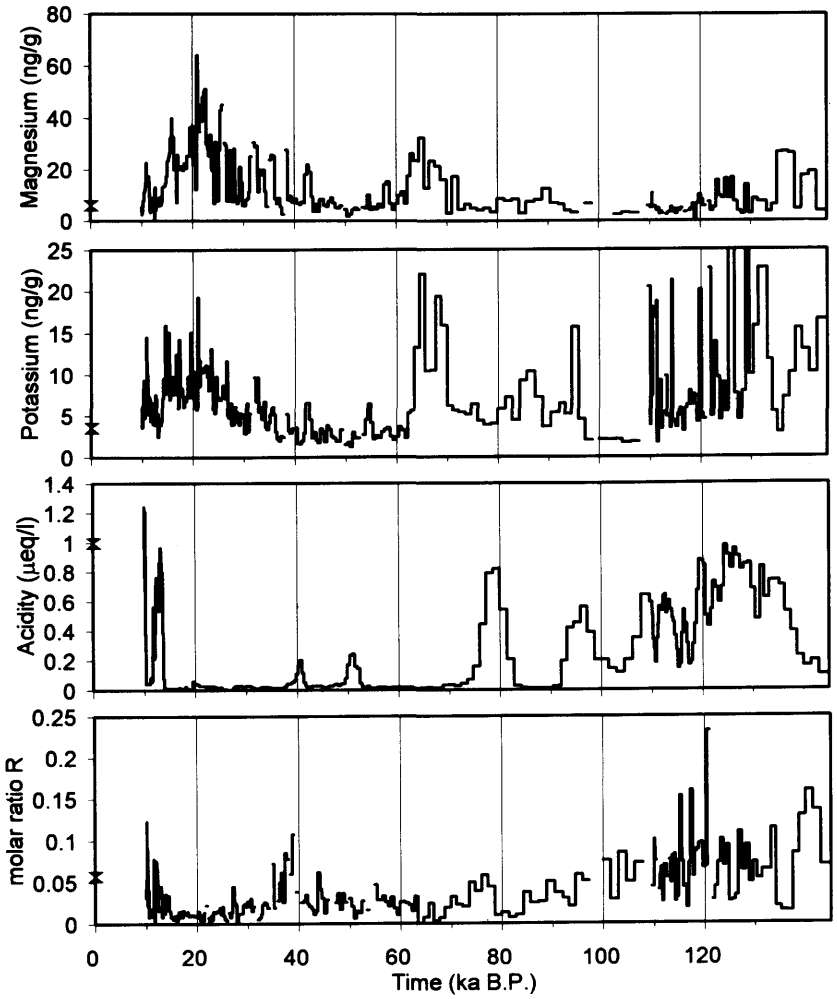

Fig. 4. (cont'd).

the mean values although they only affect the mean values of H^+ and SO_4^{2-} (the mean values for the seven years are 1.21 and 1.49 μeq/l, respectively).

The Boudinage layer represents a short time period during stage 4 but is treated separately. The stages 5a, 5b, 5c and 5d are averaged together due to the low sample resolution in this part of the record. The term stage 5e is used for the period 110–122 ka B.P.

The coming results from the two Summit ice cores will be interesting to compare with the Renland ice core ion data. So far, only the calcium profile has been reported for the full period (GRIP members, 1993) but its variations and concentration range are consistent with the Renland profile. This indicates that the results from both Renland and Summit have a large regional significance. The impurities are long range transported and the high crustal influence on Renland is not a local phenomenon attributed to the vicinity of ice free coastal areas. Concentration variations at Summit of other ions have been reported for shorter time periods, for example the variations of Ca^{2+} and NH_4^+ in the GRIP ice core (Fuhrer et al., 1993) and Ca^{2+} in the GISP2 ice core (Mayewski et al.,

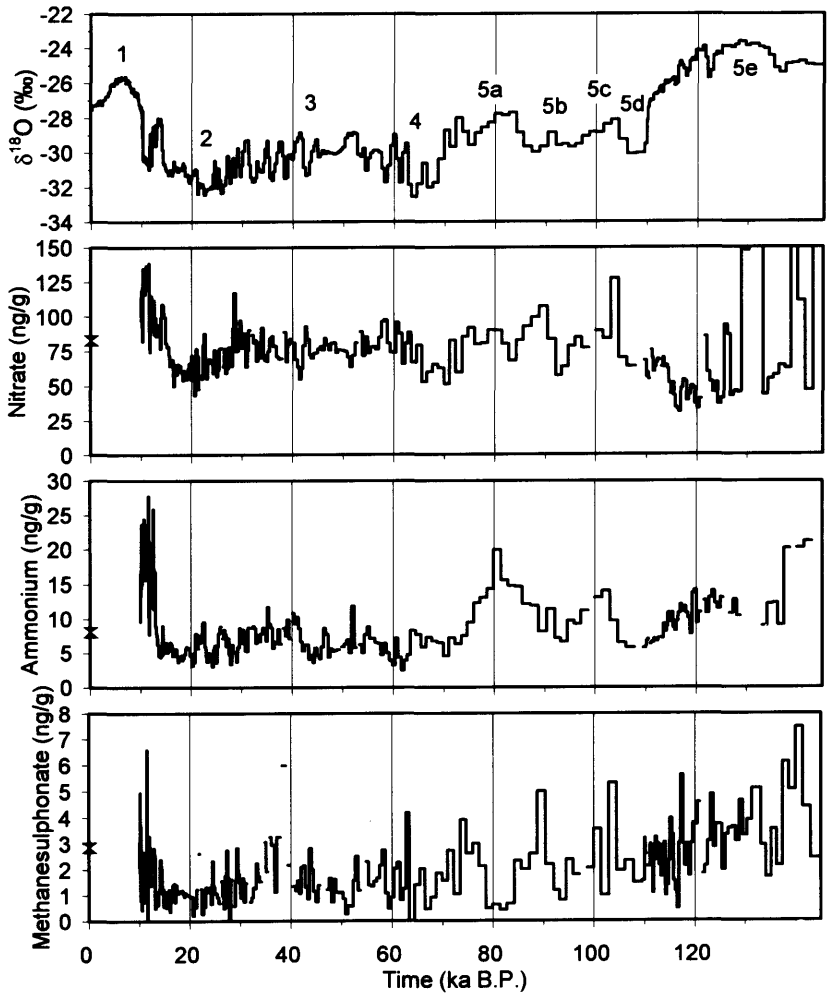

Fig. 5. The Renland ice core profiles of $\delta^{18}O$, NO_3^-, NH_4^+ and $CH_3SO_3^-$, respectively. The records are affected by melt layers beyond 122 ka B.P. The mean value of five full years in the late Holocene (A.D. 1813–1815 and 1818–1819) is indicated by a cross to the left in each figure.

1993) between the Alleröd–Bölling interstadial, the Younger Dryas event and the Pre-boreal period. The reported variations and concentration ranges are consistent with the Renland profiles, as is the reported seasonal NH_4^+ variations in the late Holocene (Legrand et al., 1992a).

Comparisons of Renland ion concentrations with previous published Greenland data from the glacial period are limited to Na^+, K^+, Mg^{2+} and Ca^{2+} measured by atomic absorption in the Camp Century ice core (Cragin et al., 1977) and Cl^-, NO_3^- and SO_4^{2-} measured by ion chromatography in the Camp Century and Dye 3 ice cores (Herron and Langway, 1985). However, the preliminary time scales on which the data were published have later been revised (Dansgaard et al., 1984). The general trends are the same in all three ice cores. Glacial concentrations are higher than pre-industrial Holocene values and maximum concentrations are found in stage 2 (revised time scales for Camp Century and Dye 3) for all ions in the comparison except NO_3^-. The decrease

in concentrations occurred rapidly during the transition to Holocene. The Renland records also shows high concentrations in stage 4. The Camp Century and Dye 3 records have low resolution in this part of the time series but high concentrations are found prior to stage 2. The concentration of NO_3^- is lower during the glacial period than in the Holocene in all three ice cores, with a sudden increase above the Holocene value prior to the transition to the Holocene.

The late Holocene concentrations of Cl^-, NO_3^- and SO_4^{2-} at Renland are, in a comparison with the full Holocene averages (Herron and Langway, 1985), roughly a factor of two higher than at Dye 3, and slightly higher than at Camp Century. However, the variations during the Holocene at Camp Century and Dye 3 are exceeding a factor of two for all three ions. Investigations of limited time periods during the Holocene have been performed on other shorter ice cores from Greenland (summarised by Clausen and Langway, 1989) which also show a variability between different locations, and between different shorter pre-industrial Holocene time periods, exceeding a factor of two. Thus, this comparison of non-identical time periods is only approximate. The late Holocene Renland concentrations of Na^+ and K^+ are only slightly higher than full Holocene averages at Camp Century (Cragin et al., 1977), but Mg^{2+} and Ca^{2+} are higher by a factor of 2.3 and 4.2, respectively.

The concentrations of Cl^-, SO_4^{2-}, Na^+, K^+, Mg^{2+} and Ca^{2+} during stage 2 are similar or lower at Renland than at the other locations. Thus, the changes in concentrations between stage 2 and the Holocene are smaller at Renland. The change in NO_3^- concentration between stage 2 and the Holocene is small and similar in all cores.

More detailed glacial records of Cl^-, NO_3^- and SO_4^{2-} in the Dye 3 ice core in selected periods with rapid climatic changes have been published by Finkel and Langway (1985). Periods with lower $\delta^{18}O$ values are associated with higher ion concentrations and the variations are larger and more distinct for SO_4^{2-} than for Cl^- and NO_3^-. This is consistent with the Renland records where NO_3^- also exhibits an anti-correlation to $\delta^{18}O$ in the fast climatic oscillations in the glacial period, although the long-term trend shows lower concentrations in colder climatic stages.

Dust and acidity have been measured in continuous profiles along the Dye 3 ice core (Hammer et al., 1985). The glacial concentrations and the fast variations in dust content in the Renland ice core are consistent with the Dye 3 record. The Renland dust content in the late Holocene is roughly a factor of two higher than the Holocene mean value at Dye 3. The alkaline conditions in Greenland ice during the glacial period have been observed in all deep ice cores and the alkalinity has been confirmed by pH measurements on melted samples from the Dye 3 ice core. The late Holocene acidity signal at Renland has a similar value as the full Holocene average at Dye 3.

5.3. *The ionic balance*

The sum of detected major anions ($\Sigma- = \{Cl^-\} + \{NO_3^-\} + \{SO_4^{2-}\}$) and cations ($\Sigma+ = \{H^+\} + \{Na^+\} + \{K^+\} + \{NH_4^+\} + \{Mg^{2+}\} + \{Ca^{2+}\}$), respectively, are given as mean values for the various climatic stages in Table 3. Also given are ΔC which is the mean value of $(\Sigma+) - (\Sigma-)$ and Σ which is the mean value of $(\Sigma+) + (\Sigma-)$. The ratio $\Delta C/\Sigma$ describes the mean imbalance in the budget. Methanesulphonate constitute less than 0.5% of the total ionic budget in all stages and has been neglected in the calculations. Fluoride was analysed (not reported here) but never found in a concentration exceeding 0.5% of the total ionic budget. The content of HCO_3^-/CO_3^{2-} (the form of the carbonate ion is dependent on the pH in the solution) was never quantified, but is thought to be important in periods with high input of crustally derived alkaline impurities (i.e., $CaCO_3$ and $MgCO_3$). The acidity in this study is measured as conductivity of the solid ice. The acidity signal represents the true deposition of strong acids (i.e., HNO_3 and H_2SO_4), probably unaffected by carbonates if present in the ice. The budget of detected anions and cations is close to balance in the Holocene periods but the concentration of NO_3^- and nss SO_4^{2-} is a factor of 2–3 higher than the acidity signal (H^+). NH_4^+ can only account for 33–50% of this discrepancy by being another counter ion than H^+ during deposition (e.g., in $(NH_4)_2SO_4$). This suggests that the rest of the NO_3^- and nss SO_4^{2-} was deposited together with Ca^{2+} and Mg^{2+} and that means that the alkaline calcium and magnesium carbonates where neutralised in the atmosphere and no carbonate was deposited. Another possibility is that the

Table 3. *The Renland ice core mean concentrations ± standard deviation ($\mu eq\ l^{-1}$)*

	Stage 1 late Holocene	Stage 1 Pre-boreal	Younger Dryas	Alleröd–Bölling
Depth (m)	86.60–89.05	305.80–306.55	306.55–307.30	307.30–308.35
Age (ka B.P.)	A.D. 1813–1819[a]	10.0–10.5	10.5–11.8	11.8–14.4
Samples (#)	35	15	15	21
$\delta^{18}O$ (‰)	−27.40 ± 1.68	−27.98 ± 0.61	−30.57 ± 0.23	−29.00 ± 0.76
Dust (ng/g)	133 ± 110	75 ± 31	530 ± 341	152 ± 86
$CH_3SO_3^-$	0.030 ± 0.016	0.025 ± 0.011	0.016 ± 0.010	0.018 ± 0.009
Cl^-	1.09 ± 0.66	0.80 ± 0.15	1.13 ± 0.11	1.18 ± 0.21
NO_3^-	1.34 ± 0.59	1.68 ± 0.16	2.03 ± 0.14	1.53 ± 0.19
SO_4^{2-}	1.14 ± 0.66	1.10 ± 0.30	1.73 ± 0.62	1.21 ± 0.34
nss SO_4^{2-}	1.03 ± 0.66	1.02 ± 0.31	1.62 ± 0.61	1.09 ± 0.33
Na^+	1.01 ± 0.60	0.96 ± 0.14	1.06 ± 0.16	1.32 ± 0.31
NH_4^+	0.45 ± 0.33	0.91 ± 0.20	1.14 ± 0.19	0.65 ± 0.32
K^+	0.09 ± 0.05	0.15 ± 0.05	0.18 ± 0.06	0.13 ± 0.04
nss K^+	0.07 ± 0.05	0.14 ± 0.04	0.16 ± 0.06	0.11 ± 0.04
Mg^{2+}	0.50 ± 0.21	0.38 ± 0.10	1.14 ± 0.36	0.55 ± 0.24
nss Mg^{2+}	0.26 ± 0.17	0.23 ± 0.10	0.93 ± 0.35	0.33 ± 0.21
Ca^{2+}	1.06 ± 0.81	0.34 ± 0.30	5.97 ± 3.12	1.51 ± 1.08
nss Ca^{2+}	1.02 ± 0.80	0.31 ± 0.30	5.93 ± 3.12	1.46 ± 1.08
H^+	1.00 ± 0.44	0.85 ± 0.30	0.05 ± 0.02	0.50 ± 0.29
Cl^-/Na^+	1.15 ± 0.28	0.84 ± 0.16	1.09 ± 0.13	0.92 ± 0.17
R (molar ratio)	0.078 ± 0.055 (0.057)[b]	0.051 ± 0.026	0.022 ± 0.016	0.035 ± 0.018
$\Sigma-$	3.56 ± 1.34	3.58 ± 0.28	4.89 ± 0.70	3.92 ± 0.49
$\Sigma+$	3.79 ± 1.28	3.53 ± 0.29	9.55 ± 3.50	4.66 ± 1.23
ΔC	0.23 ± 0.67	−0.04 ± 0.38	4.66 ± 2.90	0.74 ± 0.88
Σ	7.36 ± 2.54	7.11 ± 0.42	14.44 ± 4.14	8.57 ± 1.66
$\Delta C/\Sigma$	0.04 ± 0.08	−0.01 ± 0.05	0.29 ± 0.12	0.07 ± 0.07

[a] Except 1816–1817.
[b] Ratio between the mean values of $CH_3SO_3^-$ and nss SO_4^{2-}.

neutralisation occurred in the ice after deposition (Delmas, 1993) but if that is the case no interpretation of atmospheric compound composition is possible from ice core ionic budgets.

During glacial conditions, the acidity signal is absent (i.e., the ice is alkaline) and there is a large deficiency of anions. The glacial ionic budget is totally dominated by Ca^{2+} and the deficiency of anions is probably attributable to a carbonate contribution which has not been quantified. The concentration of NH_4^+ is low and its importance as a neutralising ion is strongly diminished. The incomplete ionic budget cannot reveal if all strong acids were neutralised in the glacial atmosphere before deposition. In milder glacial stages when the concentrations of nss Ca^{2+} and nss Mg^{2+} is close to or below Holocene values (stage 5c, stage 5a and Alleröd–Bölling), the ice is acidic and the concentration of NH_4^+ is high. H^+ and NH_4^+ are then the dominating counter ions to NO_3^- and SO_4^{2-}. However, the concentration of NH_4^+ continues to increase during the cold Younger Dryas event, although the concentration of the crustally derived impurities increases and the acidity signal is absent. Also the concentration of NO_3^- is exceptionally high during Younger Dryas (Fig. 6).

The ratio between the sea salt elements Cl^- and Na^+ is close to the bulk sea water ratio (molar ratio 1.16) in all samples in the late Holocene period, which indicates that no fractionation of the sea salt aerosol occurred nor that any additional source of Cl^- or Na^+ was present. During cold glacial stages, the ratio decreases (Table 3) which means that an excess of Na^+ is present in the ice. The excess Na^+ is found in the samples which are heavily influenced by crustally derived impurities.

Stage 2	Stage 3	Stage 4	Stage 4 Boudinage layer	Stage 5a–d	Stage 5e Eem
308.35–311.75	311.75–315.15	315.15–319.85	315.65–319.55	319.85–321.35	321.35–323.05
14.4–30.2	30.2–57.6	57.6–70.0	63.5–64.5	70.0–110.2	110.2–121.6
68	68	16	78	30	34
-31.30 ± 0.59	-30.17 ± 0.78	-30.91 ± 1.01	-32.22 ± 0.24	-28.99 ± 0.71	-25.78 ± 0.92
1109 ± 593	474 ± 424	1169 ± 804	1808 ± 348	317 ± 345	255 ± 118
0.012 ± 0.007	0.016 ± 0.008	0.017 ± 0.013	0.009 ± 0.007	0.021 ± 0.014	0.027 ± 0.014
1.30 ± 0.19	1.17 ± 0.16	1.48 ± 0.21	1.37 ± 0.24	0.95 ± 0.22	0.83 ± 0.20
1.12 ± 0.23	1.24 ± 0.13	1.24 ± 0.22	1.11 ± 0.13	1.30 ± 0.26	0.86 ± 0.20
2.17 ± 0.70	1.40 ± 0.53	2.18 ± 0.93	3.04 ± 0.60	1.24 ± 0.46	0.85 ± 0.21
2.04 ± 0.69	1.29 ± 0.53	2.03 ± 0.93	2.91 ± 0.59	1.14 ± 0.45	0.77 ± 0.20
1.32 ± 0.30	1.03 ± 0.29	1.68 ± 0.38	1.55 ± 0.36	0.86 ± 0.26	0.91 ± 0.24
0.32 ± 0.09	0.39 ± 0.10	0.31 ± 0.09	0.41 ± 0.08	0.57 ± 0.21	0.51 ± 0.12
0.21 ± 0.08	0.10 ± 0.07	0.20 ± 0.16	0.23 ± 0.13	0.15 ± 0.10	0.20 ± 0.14
0.19 ± 0.08	0.08 ± 0.07	0.17 ± 0.16	0.21 ± 0.13	0.13 ± 0.10	0.18 ± 0.13
2.07 ± 1.00	0.86 ± 0.64	1.27 ± 0.65	2.70 ± 0.69	0.50 ± 0.27	0.39 ± 0.18
1.82 ± 0.98	0.64 ± 0.63	0.99 ± 0.63	2.44 ± 0.69	0.32 ± 0.27	0.23 ± 0.19
9.71 ± 5.39	3.79 ± 4.67	8.20 ± 6.52	17.70 ± 4.18	1.74 ± 2.21	0.60 ± 0.46
9.66 ± 5.39	3.74 ± 4.67	8.15 ± 6.52	17.64 ± 4.18	1.70 ± 2.21	0.57 ± 0.46
0.02 ± 0.01	0.04 ± 0.05	0.02 ± 0.01	0.01 ± 0.00	0.27 ± 0.24	0.46 ± 0.19
1.01 ± 0.15	1.20 ± 0.28	0.91 ± 0.15	0.91 ± 0.13	1.13 ± 0.20	0.93 ± 0.18
0.014 ± 0.009	0.026 ± 0.014	0.020 ± 0.011	0.006 ± 0.005	0.040 ± 0.024	0.074 ± 0.043
4.58 ± 0.89	3.81 ± 0.70	4.89 ± 1.02	5.52 ± 0.75	3.49 ± 0.75	2.53 ± 0.50
13.64 ± 6.64	6.15 ± 5.49	11.68 ± 7.62	22.59 ± 4.79	4.03 ± 2.43	3.03 ± 0.75
9.05 ± 5.85	2.34 ± 4.88	6.78 ± 6.67	17.07 ± 4.48	0.54 ± 1.90	0.50 ± 0.67
18.22 ± 7.46	9.96 ± 6.13	16.57 ± 8.59	28.11 ± 5.19	7.52 ± 3.05	5.57 ± 1.08
0.43 ± 0.19	0.09 ± 0.25	0.29 ± 0.26	0.60 ± 0.06	0.02 ± 0.16	0.08 ± 0.11

The excess Na^+ is 17% and 24% of the total Na^+ concentration in stage 2 and 4, respectively. The mean ratio between Cl^- and Na^+ never exceeds the sea water ratio for any climatic stage, i.e., never indicating an excess of Cl^-, which is a further indication that the deviation from the sea water ratio is due to an additional (crustal) source of Na^+ and not a fractionation process in the atmosphere between the sea salt elements.

5.4. *Seasonal variations*

The late Holocene time series have the highest sample resolution, 5–9 samples per year, which is sufficient to reveal seasonal variations of deposition. The ionic budget for this period is in balance. The concentration profiles (Fig. 7), expressed as μeq/l, may thus reveal the compounds in which the ions are deposited. The sea salt elements Cl^- and Na^+ form one group with large seasonal differences and maximum concentrations during winter. Maximum concentrations of NO_3^-, nss SO_4^{2-} and H^+ are found during spring and summer (the concentrations of nss SO_4^{2-} and H^+ are enhanced during A.D. 1816 and 1817 due to the volcano Tambora eruption in A.D. 1815). The profile of NH_4^+ follows the $\delta^{18}O$ profile with the highest concentrations during summer, sometimes later than NO_3^-, nss SO_4^{2-} and H^+. The profiles of nss Ca^{2+}, nss Mg^{2+} and nss K^+ have sporadic high peaks predominantly during the colder part of the year. The variations in these records (not identical) are nevertheless following the patterns of NO_3^- and nss SO_4^{2-} which indicates that all of them can be counter ions to nss SO_4^{2-} and NO_3^- during deposition. The seasonal patterns of $CH_3SO_3^-$ are not clear but the highest concentrations are always found during the colder part of the year and low concentrations during summer. The dust profile shows the highest concentrations during fall and winter. The dust profile is closely related to the profile of nss Ca^{2+}. Similarities are also found between the profiles of dust and

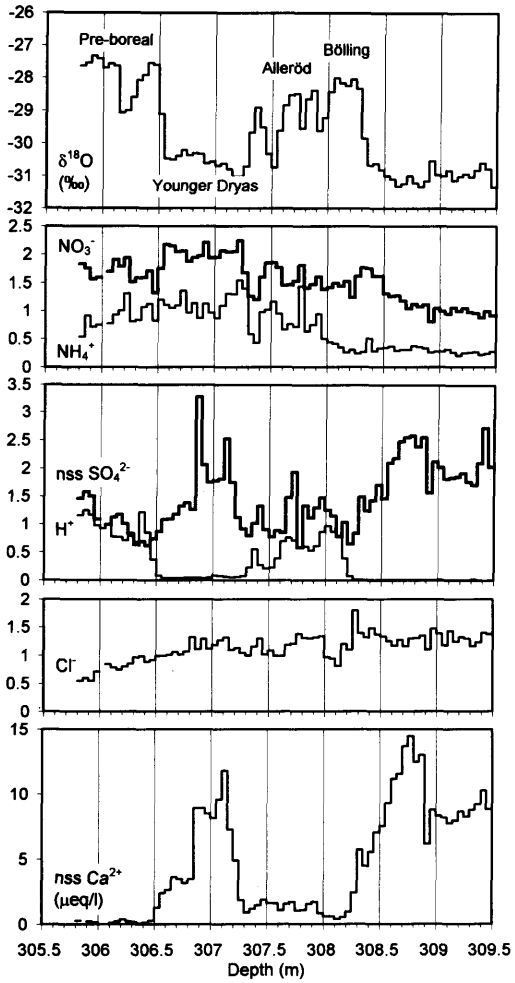

Fig. 6. The Renland ice core profiles of $\delta^{18}O$ and nitrate, ammonium, nss sulphate, acidity, chloride and nss calcium, respectively, on a linear depth scale covering the fast climatic variations of the periods Bölling, Allerød, Younger Dryas and Pre-boreal. The ion concentrations are expressed in $\mu eq\ l^{-1}$.

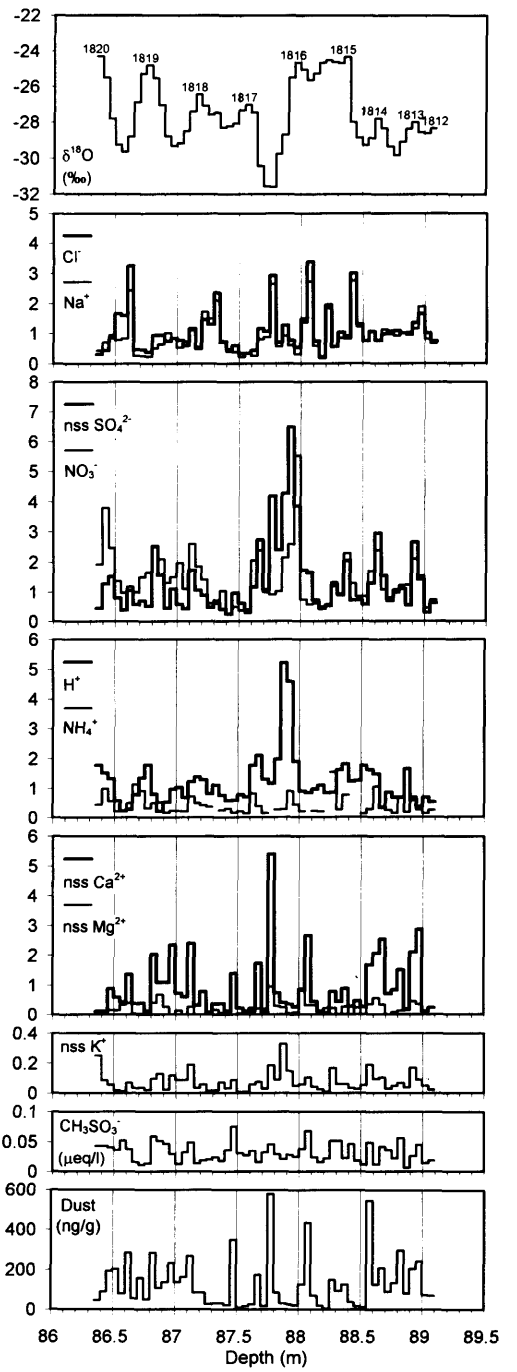

Fig. 7. The Renland ice core profiles of $\delta^{18}O$, dust and all analysed ions on a linear depth scale covering the time period A.D. 1812–1820 (the late Holocene time series). The ion concentrations are expressed in $\mu eq\ l^{-1}$. Low $\delta^{18}O$ values represent winter precipitation.

$CH_3SO_3^-$. The sea salt contribution, estimated from the Cl^- concentration, is on average 12% of the total concentration of SO_4^{2-}, 7% of Ca^{2+}, 51% of Mg^{2+} and 27% of K^+ in the late Holocene period.

5.5. *The distribution between soluble and insoluble impurities*

The soluble impurity fraction represents 65% of the total mass of impurities in the late Holocene

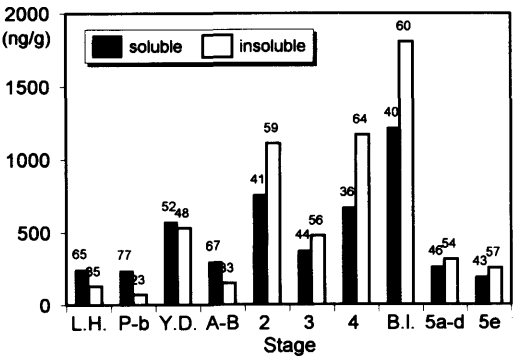

Fig. 8. The distribution between soluble and insoluble impurities in each climatic stage. The deficient anions in glacial stages (see ΔC in Table 3) are assumed to have the molar mass of carbonate (CO_3^{2-}).

and the insoluble fraction (dust) represents 35% (Fig. 8). Although the total concentrations are varying considerably between the various climatic stages, the distribution between soluble and insoluble impurities is roughly 40% soluble mass and 60% insoluble mass in all stages from stage 5e to stage 2. During the Alleröd–Bölling, the relative contribution shifts to 67% soluble and 33% insoluble impurities and the soluble impurities are in a majority in all following periods. The deficiency of anions (i.e., a positive ΔC in Table 3) had to be accounted for in this comparison since it represents a large fraction of the soluble impurities in some stages. The deficient anions were assumed to have the molar mass of CO_3^{2-} when the total mass of soluble impurities was calculated.

6. Discussion

If we want to establish a record of the past atmospheric aerosol, the parameter possible to measure is the concentration of different impurities in ice sheets and ice caps. The impurity concentration profiles in the ice are functions of airborne concentrations and the total scavenging (by wet and dry deposition). In general on Greenland, wet deposition is the dominant deposition process but dry deposition may be important in periods with low snow accumulation rates. Estimates of wet and dry deposition suggest that dry deposition is negligible for submicron species such as SO_4^{2-} at Dye 3 under present conditions, while dry deposition may account for roughly 30% of the total content of crustally derived components in the snow on a year-round basis (Davidson et al., 1993).

The airborne concentrations on Greenland depend on the sources (strengths and locations), the atmospheric residence times of the impurities and the transit time of air parcels from the source areas to Greenland. The pattern of the general circulation of the atmosphere, probably changing between glacial and interglacial conditions (COHMAP, 1988; Joussaume, 1993), determines which source areas are influencing Greenland. The transit time of air parcels was probably shorter (provided that the distance to the influencing source area was identical) during the glacial period due to a stronger general circulation of the atmosphere when the latitudinal temperature contrasts were larger. The residence times of the impurities in the atmosphere are determined by wet and dry deposition and chemical transformation processes along the transport path to Greenland. The residence times were probably longer during the glacial period as an effect of the lower water vapour capacity in a colder atmosphere and hence a lower wet scavenging rate of the impurities. On the other hand, a stronger general circulation of the atmosphere may have lead to more frontal cyclones with more precipitation events and a more efficient scavenging. This is neglected in the following discussion, as are possible effects of changes in chemical transformation processes due to a different composition of the atmospheric aerosol.

A simple model involving the parameters discussed above is formulated to examine the importance of changes in the hydrological cycle and the general circulation of the atmosphere. The variations in concentrations in the ice and deposition fluxes are studied. First, in the following sections, the source types of different impurities are summarised to reveal possible connections (e.g., due to same source or same size of the impurities). Next, the estimates of accumulation rate changes are discussed. The accumulation rate is essential to be able to calculate deposition fluxes. Finally, the simple model is described and the model results are evaluated.

6.1. Sources of impurities

The main sources likely to contribute to the impurity concentrations in the Renland ice core

are summarised in Table 4. The impurities are divided into 5 major groups according to their origin from marine and terrestrial sources, subdivided into biogenic and non-biogenic sources, and atmospheric sources. Most impurities have more than one source. A review of publications dealing with sources influencing impurity concentrations in polar ice cores are found in Mayewski et al. (1992).

The first column contains one marine non-biogenic source, i.e., sea salt. The sea salt contribution to the concentrations of Cl^-, SO_4^{2-}, Na^+, K^+, Mg^{2+} and Ca^{2+} comes from sea spray. The generated droplets create coarse mode aerosol particles on drying which act as cloud condensation nuclei (CCN). The number concentration of sea salt particles is normally low compared to a fine mode aerosol of the same total mass.

The second column contains the marine biogenic source of $CH_3SO_3^-$ and SO_4^{2-}, i.e., oxidation of dimethyl sulphide (DMS). Also NH_4^+ from degrading organic material may be emitted from the ocean (Quinn et al., 1988). DMS is emitted from phytoplankton in the ocean and oxidised in the atmosphere by hydroxyl radicals to methanesulphonic acid (MSA) and sulphur dioxide (SO_2), the latter oxidised further to SO_4^{2-}. MSA is highly soluble and dissolves rapidly in droplets in the atmosphere. SO_2 can be oxidised by a multistep gas-phase reaction (Calvert et al., 1978) and thus form new CCN in the fine mode size range or be oxidised in the aqueous phase (Penkett et al., 1979) and become associated with pre-existing particles. This latter process does not produce new CCN but by modifying the size distribution of the aerosol additional particles may be activated at a given supersaturation (Hegg, 1990). The aqueous phase oxidation is generally thought to dominate in the present atmosphere. MSA has attracted attention as a possible tracer of biogenic sulphur emissions since DMS oxidation is the only known source of MSA. A temperature dependency of the branching ratio R ($CH_3SO_3^-$/nss SO_4^{2-} molar ratio) has been inferred (Berresheim, 1987) from laboratory oxidation studies (Hynes et al., 1986) of the reaction of DMS with OH. A latitudinal gradient of R in marine aerosol particles have been observed (Bates et al., 1992a) with higher ratios associated with higher latitudes, and thus lower temperatures, in accordance with the result of the laboratory studies. The magnitude of R at Cape Grim, Tasmania (Ayers et al., 1991) has been found to decrease during winter, which indicates that other factors apart from the temperature can control R measured in situ (e.g., seasonal transport differences, additional sources of nss SO_4^{2-}, composition of pre-existing aerosol etc.). Accordingly, the use of $CH_3SO_3^-$ in polar precipitation as a quantitative tracer of biogenic sulphur emissions over long time periods with different climatic conditions (like glacial and interglacial conditions) demands caution since the ratio R then most probably is affected by several other conditions than temperature (Hansson and Saltzman, 1993). However, the R values found at Renland are showing a linear relationship

Table 4. *Main sources of impurities in the Renland ice core*

	Marine sources		Terrestrial sources		Atmospheric sources
	non-biogenic	biogenic	non-biogenic	biogenic	
Dust			W		
$CH_3SO_3^-$		D		(D)	
Cl^-	SS		(V)		
NO_3^-				M, B	SI, L
SO_4^{2-}	SS	D	V, W	(D), M, B	SI
Na^+	SS		W		
NH_4^+		DO		M, B	
K^+	SS		W	B	
Mg^{2+}	SS		W		
Ca^{2+}	SS		W		

Sea salt (SS), DMS oxidation (D), Degrading organic material (DO), Volcanic emissions (V), Weathering and wind suspension (W), Microbial processes (M), Biomass burning (B), Stratospheric input (SI), Lightning (L). Sources known to have a small effect on the concentrations are put in parentheses.

($r^2 = 0.99$) with the $\delta^{18}O$ values when plotted as mean values for the different climatic stages (Fig. 9), but with lower ratios associated with colder climatic stages.

The third column contains two terrestrial non-biogenic sources, i.e., weathering and wind suspension and volcanic emissions. Weathering followed by suspension by wind of crustal material gives the insoluble fraction, i.e., dust. The soluble fraction from this source is dominated by Ca^{2+}, Mg^{2+} and CO_3^{2-}. A crustal contribution may also be seen in the concentrations of SO_4^{2-}, Na^+ and K^+, depending on the crustal composition. The weathering products are mainly coarse mode particles (larger than the sea salt aerosol). They act as CCN and the droplets can effectively dissolve and neutralise acidic gases due to their alkaline character.

Emissions from both erupting and non-erupting degassing volcanoes contribute to the concentration of SO_4^{2-}. The explosivity of the eruptions determines the distance to where they leave traces in the precipitation. The largest, explosive eruptions can inject SO_2 into the stratosphere and thus have an effect on the sulphate concentration in both hemispheres for several years. Degassing volcanoes have been estimated to account for 36% of the volcanic SO_2 on a global basis (Stoiber et al., 1987). Continuously degassing volcanoes contribute to the background concentration while emissions from explosive eruptions enhance the concentrations for a few years. Only the contribution from explosive eruptions can be distinguished from sulphate of other origin, and then only by its suddenness and short duration. The sample resolution in this study (except for the late Holocene period) is too coarse to reveal the influence of individual, explosive eruptions. Model studies (Langner, 1991) of the distribution of tropospheric sulphate indicate an increasing importance of volcanic sulphate with altitude and thus an increasing relative influence on the concentration in the precipitation at higher altitudes. This is due to the fact that volcanic emissions in general are introduced to the atmosphere at higher altitudes than the marine biogenic emissions at sea level. The possible contribution of Cl^- in the form of HCl from some erupting volcanoes cannot be detected in samples with a time resolution of at best a hundred years as is the case with the Renland ice core samples from the glacial period. Neither are traces of volcanic Cl^- from the Tambora eruption found in the late Holocene samples in accordance with previous ice core analyses of that specific eruption (Clausen and Hammer, 1988; Langway et al., 1988).

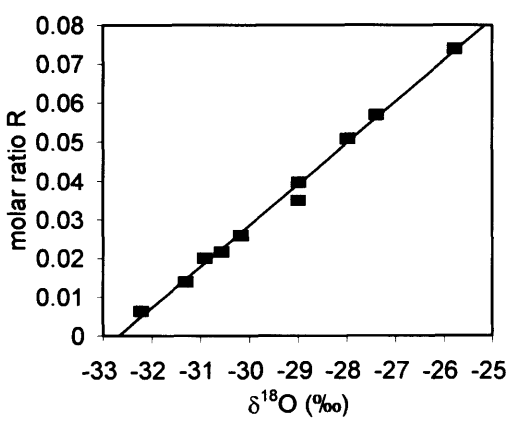

Fig. 9. Plot of the molar ratio R ($CH_3SO_3^-$/nss SO_4^{2-}) against the mean $\delta^{18}O$ value in each climatic stage ($r^2 = 0.99$). The ratios are mean values of the individual ratios except for the late Holocene time series where the ratio is calculated from the mean values of $CH_3SO_3^-$ and nss SO_4^{2-} to reduce the influence of the seasonal variations in the ratio.

The fourth column contains terrestrial biogenic sources such as microbial processes in wetlands, soils and vegetation and biomass burning causing emissions of nitrogen oxides (NO_x), ammonia (NH_3) and reduced sulphur compounds (e.g., H_2S and DMS). Biomass burning may also add to the concentration of K^+. The reduced sulphur compounds are oxidised via SO_2 to SO_4^{2-}. A small fraction of the DMS is oxidised to $CH_3SO_3^-$ but is assumed to be negligible compared to the marine biogenic contribution. The nitrogen oxides are oxidised in several steps to gaseous nitric acid (HNO_3) which dissolves rapidly in droplets in the atmosphere. The chemistry of nitrogen compounds in the atmosphere is complex and the knowledge about sources, sinks and distribution is at present limited. NH_3 is an alkaline gas, which dissolves rapidly in acidic droplets forming ammonium ions (NH_4^+) but remains as a gas if the pre-existing aerosol is alkaline.

The fifth column contains atmospheric sources such as fixation of nitrogen in the troposphere by lightning, stratospheric input of nitric acid (N_2O from bacterial action at the surface of the Earth

but oxidised in the stratosphere) and the input of a stratospheric sulphate aerosol (terrestrial biogenic CS_2 and OCS oxidised in the stratosphere and volcanic sulphate).

It is difficult to estimate the source strength of natural sources of today. It is even more difficult to apportion how different sources influence the ion concentrations in the precipitation in a specific receptor area, especially for the precipitation in the past. Sulphate has a variety of sources but it is also the ion that is most studied. Present estimates for the sulphur emissions in the NH from different natural sources suggest that volcanic emissions contribute with 46% of the total natural sulphur, marine biogenic emissions 44%, biomass burning 8% and terrestrial biogenic emissions 2% (Bates et al., 1992b). Similar numbers are given by Spiro et al. (1992). The contribution from biogenic sources is strongest at lower latitudes while volcanic contributions are more equally distributed in the NH. The situation in the SH is quite different from the NH. The marine biogenic emissions are estimated to be 40% larger in the SH and the other emissions are smaller, which makes the marine biogenic emissions to account for 70% of the total natural sulphur budget in the SH.

6.2. Accumulation rates

The accumulation rates on Greenland have changed markedly between glacial and interglacial conditions. The change is similar all over Greenland and thus probably largely determined by the higher water vapour capacity in warm air than in cold air, which thus can allow higher precipitation rates. Changes in the low pressure tracks and thus the frequency of snowfalls may have influenced the accumulation rates more locally. One estimate of the accumulation rate at Renland was derived as an output parameter by tuning the ice flow model used for dating the ice core so as to reproduce the well known dates of easily identifiable features in the $\delta^{18}O$ record (Johnsen and Dansgaard, 1992). The accumulation rate was estimated to be constant during the Holocene (50 cm ice equivalent per year), 40% of present accumulation rate during the Younger Dryas and Alleröd–Bölling, 22% during stage 2, 3 and 4, 30% during stage 5a–d and 120% during stage 5e. This is a rough estimate and the accumulation rate was probably changing largely and abrupt within these periods, as was the temperature. A doubling in accumulation rate within one to three years in the end of the Younger Dryas event has been interpreted from the GISP2 ice core (Alley et al., 1993).

Changes in accumulation rate can also be estimated from the concentration of the radioisotope ^{10}Be in polar ice. The concentration of ^{10}Be has been measured in the Camp Century ice core (Beer et al., 1988). Due to the low time resolution, this record does not either reveal the fast variations in accumulation rate. However, the magnitude of the concentration change of ^{10}Be between glacial maximum and interglacial conditions is consistent with the estimate of a changed accumulation rate by a factor of 4 to 5.

The estimated accumulation rate in each climatic stage is plotted against the mean $\delta^{18}O$ value (Fig. 10). An exponential relationship is approximated to these few points to achieve a somewhat better estimate for the different stages. This exponential approximation is used in the deposition flux calculations and in the model simulation. An exponential relationship between accumulation rate and $\delta^{18}O$ values was introduced in the time scale calculations for the GRIP ice core (Dansgaard et al., 1993) where data from both interglacial and glacial conditions were used. A constant accumulation rate change with 14.4% per $^{o}/_{oo}$ $\delta^{18}O$ change was found at Summit. Two thirds of this change can be due to the higher water vapour capacity in the warm air, while the fre-

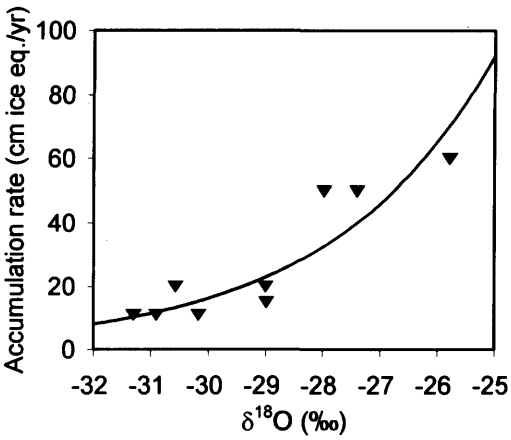

Fig. 10. Plot of the estimated accumulation rate against the mean $\delta^{18}O$ value in each climatic stage. The exponential approximation is used in the deposition flux calculations and in the model simulation.

quency of precipitation events probably accounts for the rest of the change. The exponential approximation in Fig. 10 represents an accumulation rate change with roughly 30% per $^{o}/_{oo}$ $\delta^{18}O$ change. The larger change for the Renland data is expected since the change in $\delta^{18}O$ at the transition from the glacial period to Holocene, and between mild and cold conditions during the glacial period, is lower at Renland than at the main ice sheet for reasons (i.e., diffusion of isotopic components in the ice and orographic mechanisms of precipitation) discussed by Johnsen et al. (1992a).

6.3. *Calculated deposition fluxes*

Total deposition fluxes (Φ_{tot}) are calculated from the concentrations in the ice and the accumulation rates derived from the exponential approximation with the $\delta^{18}O$ values in Fig. 10. Mean total deposition fluxes in each climatic stage are presented in Table 5. The total flux can be approximated with the wet flux (Φ_{wet}) for those impurities with insignificant dry deposition, while Φ_{tot} will exceed Φ_{wet} for the others.

The concentrations and fluxes relative to the late Holocene values for each impurity are plotted versus the mean $\delta^{18}O$ value in each climatic stage (Fig. 11). The mean $\delta^{18}O$ value should be interpreted as describing a mean climate at Renland over a long time period, thus determined by a general climate change in the NH but not necessarily representative of the NH. The impurities can be divided into three groups according to the general trends in the change of concentrations and fluxes. Dust, nss Ca^{2+} and nss Mg^{2+} show strongly increasing concentrations (up to a factor of ten) and increasing fluxes with a colder climate. Cl^-, Na^+ and nss SO_4^{2-} show moderately increasing concentrations (up to a factor of two) and decreasing fluxes. The scattered patterns of nss K^+ are in between these two groups. The concentration increases up to a factor of three but the flux shows a decreasing trend. The flux of dust and nss K^+ in stage 5e (i.e., the warmest period) is exceptionally high. The different patterns of the crustally derived ions indicates that the composition of the crustal impurities is altered between the different climatic stages. Thus, it cannot be approximated with a mean crustal composition similar for all stages. The third group contains NO_3^-, NH_4^+ and $CH_3SO_3^-$. Methanesulphonate shows clearly a decrease in both concentration and flux. The concentrations of the nitrogen compounds are not systematically changing with the climate although a weak trend of decreasing concentrations with a colder climate can be found. However, the fluxes are clearly decreasing with a colder climate.

6.4. *The model*

6.4.1. Description. The loss of a contaminant with an airborne concentration C_{air} (M/L^3) may be described as a first order process defined by the scavenging rate ψ $(1/T)$:

$$dC_{air}/dt = -\psi C_{air}. \quad (1)$$

By solving eq. (1), the change in airborne concentration with time can be described by:

$$C_{air} = C(0)_{air} \exp(-\psi t) \quad (2)$$

Table 5. *The Renland ice core mean total deposition fluxes (mg m^{-2} yr^{-1})*

	Stage 1 late Holocene	Stage 1 Pre-boreal	Younger Dryas	Alleröd-Bölling	Stage 2	Stage 3	Stage 4	Stage 5a–d	Stage 5e Eem
$\delta^{18}O$ ($^{o}/_{oo}$)	−27.40	−27.98	−30.57	−29.00	−31.30	−30.17	−30.91	−28.99	−25.78
A (cm ice eq/yr)	40	33	13	23	10	15	12	23	70
Dust	53	25	71	35	115	72	138	73	179
$CH_3SO_3^-$	1.1	0.9	0.2	0.4	0.1	0.2	0.2	0.5	1.8
Cl^-	16	9.2	5.4	9.6	4.8	6.3	6.2	7.8	21
NO_3^-	33	34	17	22	7.2	12	9.1	19	37
nss SO_4^{2-}	20	16	10	12	10	9.4	11	13	26
Na^+	9.2	7.2	3.2	7.0	3.1	3.6	4.6	4.6	15
NH_4^+	3.2	5.4	2.8	2.7	0.6	1.1	0.7	2.7	6.4
nss K^+	1.1	1.8	0.8	1.0	0.8	0.5	0.8	1.2	4.9
nss Mg^{2+}	1.3	0.9	1.4	0.9	2.3	1.2	1.4	0.9	2.0
nss Ca^{2+}	8.0	1.9	16	6.7	20	11	19	7.8	7.9

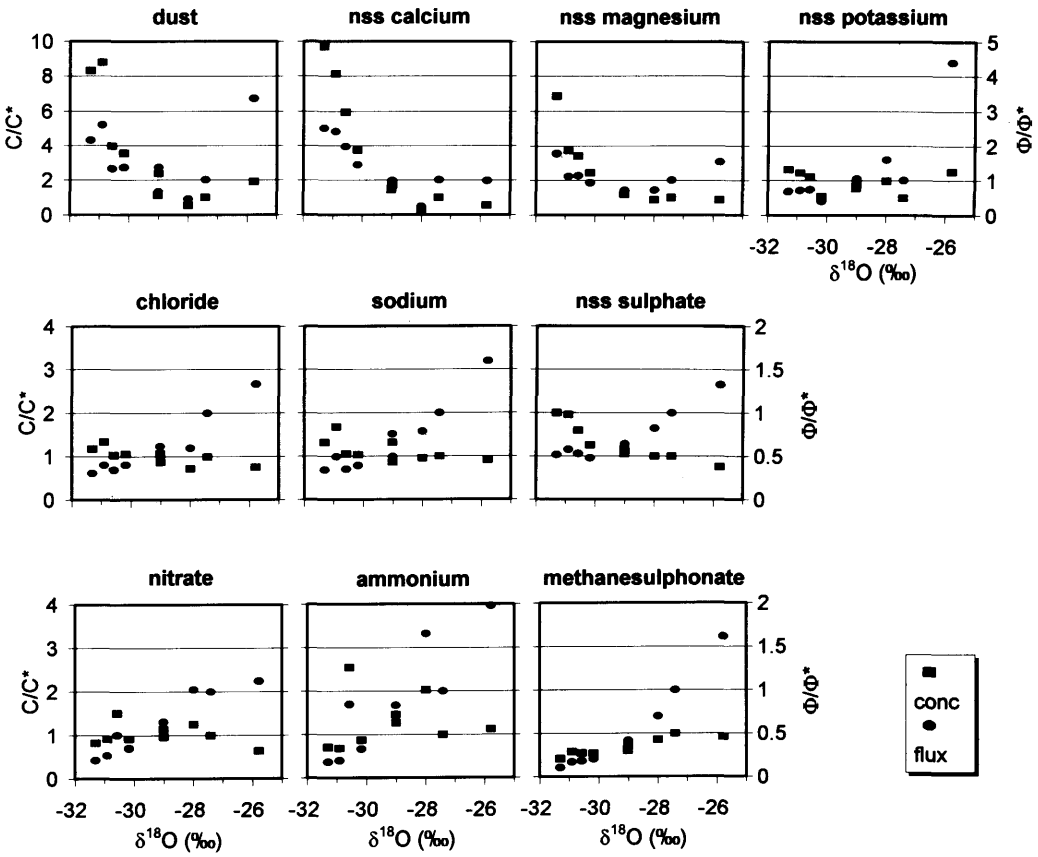

Fig. 11. Observed mean concentrations in the ice (C_{ice}/C^*_{ice}) and mean total deposition fluxes (Φ_{tot}/Φ^*_{tot}) at Renland relative to the late Holocene values, respectively, plotted against the mean $\delta^{18}O$ value in each climatic stage.

if ψ is constant. C_{air} is the airborne concentration in the moving air parcel and $C(0)_{air}$ is the airborne concentration at the source. The average residence time τ is defined by $\tau = 1/\psi$, thus giving the expression:

$$C_{air} = C(0)_{air} \exp(-t/\tau). \quad (3)$$

Eq. (3) shows how the airborne concentration at any location is dependent on the airborne concentration at the source, the transit time from the source and the residence time which may all vary with the climate. What is required is the airborne concentration at Renland in different climatic stages under the influence of changes in all of these parameters. Without knowing the absolute airborne concentration, the concentration relative to a reference state (denoted by an asterisk) can be calculated from:

$$C_{air}/C^*_{air} = C(0)_{air}/C(0)^*_{air} \exp[(1-n/k)\, t^*/\tau^*], \quad (4)$$

where $(C(0)_{air}/C(0)^*_{air})$ is the relative airborne concentration at the source and thus reflects the change in source strength, n is the relative transit time (t/t^*) and k is the relative residence time (τ/τ^*). The late Holocene climate (i.e., $\delta^{18}O = 27.4‰$) is chosen as the reference state in the following discussion.

The concentration in the ice at Renland, C_{ice} (M/M), can be approximately related to the airborne concentration at Renland according to:

$$C_{ice} = (C_{air}/C^*_{air})(W/W^*)\, C^*_{ice}, \quad (5)$$

where W/W^* is the relative local scavenging ratio at Renland. W is defined as $\rho_{air} C_{ice}/C_{air}$ where ρ_{air} (M/L^3) is the air density. The wet flux at Renland, Φ_{wet} (M/L^2T), is derived from:

$$\Phi_{wet} = (C_{air}/C^*_{air})(W/W^*)(A/A^*)\,\Phi^*_{wet}, \qquad (6)$$

where A (L/T) is the accumulation rate at Renland. The concentration in the ice and the total deposition flux ($\Phi_{tot} = \Phi_{wet} + \Phi_{dry}$) are the quantities that have been measured (or calculated from measurements). Dry deposition is assumed to be negligible at Renland for all impurities except those that are crustally derived. Thus, Φ_{tot} is larger than Φ_{wet} for the latter impurities while Φ_{tot} can be approximated with Φ_{wet} for the others. C_{ice}/C^*_{ice} can be approximated with C_{air}/C^*_{air} if W/W^* set to unity (see Subsection 6.4.3.).

6.4.2. Climate change influence. Different climatic stages are characterised by different temperatures and thus significantly different precipitation rates (as discussed as accumulation rates at the Renland ice cap in Subsection 6.3). The flux of a contaminant by wet deposition can be described by:

$$\Phi_{wet} = \rho_{water} C_{prec} P \qquad (7)$$

where ρ_{water} (M/L^3) is the water density, C_{prec} (M/M) is the concentration in the precipitation and P (L/T) is the precipitation rate. The mass scavenged can also be calculated by integration of eq. (1). By assuming that the aerosol is well mixed up to the cloud elevation H, the integral can be solved and conservation of mass consequently gives:

$$\rho_{water} C_{prec} P = \psi C_{air} H. \qquad (8)$$

The residence time ($\tau = 1/\psi$) can thus be related to the precipitation rate as follows:

$$\tau = (\rho_{air} H)/(WP\rho_{water}). \qquad (9)$$

Neglecting possible changes in H and W, the change in the residence time between different climatic stages is inversely proportional to changes in P. The effect of a possible change in W is discussed below. The average residence time is dependent on the precipitation rates along the transport path which may change by different degrees. The decrease in water vapour capacity in cold stages will be largest at high latitudes because the strongest temperature decrease is found there. The maximal change of the accumulation rate at Renland is estimated to be a decrease to roughly 20% of the Holocene value. An overall decrease of P to 20% of the Holocene values along the transport path corresponds to a factor of 5 increase of τ. Thus, the maximum value of k is set to 5 in the coldest stage and the gradual change of τ with climate is set inversely proportional to the accumulation rate at Renland. Only changes in wet deposition fluxes are considered here although some impurities are influenced by dry deposition close to the sources. Since dry deposition fluxes are quite independent of changes in P, the actual change of τ for these impurities will be less than the estimated maximal change of a factor of 5.

A stronger latitudinal temperature gradient in cold stages may lead to a stronger general circulation of the atmosphere. Shorter transit times of air parcels from influencing source areas can thus be expected in cold stages provided that the distances to influencing source areas are constant. We cannot exclude that completely different source areas are influencing Greenland in cold stages or that the distances to the same influencing source areas are changed due to different patterns of the general circulation. However, lacking this information, n is assumed to decrease with decreasing temperatures. The minimum value of n in the coldest stage is set to 0.5, which is comparable to a doubling in mean wind speed. The gradual change of n with climate is set proportional to the temperature at Renland. This gives that the ratio n/k will always decrease with decreasing temperatures and the maximal expected change gives the ratio $n/k = 0.1$ in the coldest stage.

6.4.3. Variable scavenging ratios. Only a weak inverse dependency of the scavenging ratio W on P has been found for sulphate in cold clouds by in situ measurements (Scott, 1981; Barrie, 1985a). The scavenging rate ψ has been shown by theory to be directly proportional to P for different kinds of expected ice nuclei (Slinn, 1984), supported with experimental data on silver iodide. The air parcels may experience both warm and cold clouds during the transport to Greenland. Assuming that the weak inverse dependency of W on P is valid for all impurities in all kinds of clouds, only a small effect on the residence time can be expected from changes in W. The possible effect is counteracting

the effect of a decrease in P therefore the actual change in τ may be smaller but not larger than the estimated maximal change by a factor of 5.

More important is the effect of a variable local scavenging ratio at Renland for the relationship between the concentration in the ice and the airborne concentration at Renland (eq. (5)). W in cold clouds may be dependent on the temperature due to the effect of riming (i.e., growth of ice crystals by accretion of supercooled liquid water droplets which will increase the scavenging ratio). The amount of riming is expected to decrease with the amount of liquid water in the cloud (absent at temperatures below -40°C). Variations in W between rimed and unrimed snow of about one order of magnitude have been reported (Scott, 1981; Barrie, 1985b). However, W for unrimed snow showed a stronger inverse dependency on P than rimed snow, which implies that the combined effect on W of a decrease in both temperature and precipitation rate at Renland when going from a warmer to a colder climate can be expected to be small.

6.4.4. Exploration of range. The model has been tested for various combinations of the parameters t^*/τ^*, n, k, $C(0)_{air}/C(0)^*_{air}$ and W/W^*. The magnitude of the change in n/k is more important the larger the ratio t^*/τ^* (Fig. 12). The maximal change ($n/k = 0.1$) will increase the airborne concentrations at Renland in the coldest stage by a factor of ten if the ratio t^*/τ^* is 2.5. No impurity concentration in the ice increases more than a factor of 10 therefore only values of t^*/τ^* below 2.5 are considered. The results of only a change in the ratio n/k (to 0.1 in stage 2) for four different t^*/τ^* is shown in Fig. 13 ($C(0)_{air}/C(0)^*_{air}$ and W/W^* are kept constant). Values of t^*/τ^* below 0.75 give similar results for all likely changes in n/k. The concentration in the ice increases slightly (by less than a factor of two) and the wet deposition flux decreases with a colder climate. In the range between 1.0 and 2.5 the concentration will increase strongly with a colder climate, more with a larger change in n/k, and the flux tends to increase. The change in n/k can be expected to be general for all impurities while the ratio t^*/τ^* is individual for each impurity. The degree of change in concentration and flux for each impurity when the same change in n/k is used may thus indicate possible differences in t^*/τ^*.

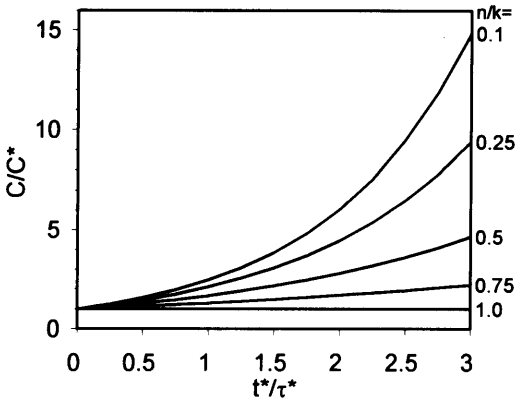

Fig. 12. The relative airborne concentration (C_{air}/C^*_{air}) against the ratio between the transit time and the residence time in the reference state (t^*/τ^*) for different changes of the ratio between the relative transit time and the relative residence time (n/k).

A decrease in the airborne concentration at the source with decreasing temperature ($C(0)_{air}/C(0)^*_{air} < 1$) or a decrease in the local scavenging ratio at Renland ($W/W^* < 1$) can counteract the effect of a large change in n/k (or the choice of a too high ratio of t^*/τ^* in the model simulation). An increase in the airborne concentration at the source with decreasing temperature ($C(0)_{air}/C(0)^*_{air} > 1$) or an increase in the local scavenging ratio at Renland ($W/W^* > 1$) will add to change (i.e., act in the same direction as a decrease in the ratio n/k). Thus, changes in $C(0)_{air}/C(0)^*_{air}$ and W/W^* cannot be excluded by comparing the patterns of measured concentrations and fluxes (Fig. 11) with the results from the model simulation (Fig. 13) since the exact values of t^*/τ^* and n/k are unknown. However, any changes in source emissions will be seen as individual changes in the patterns for each impurity while physical changes in the atmosphere will change the patterns for all of them systematically. The characteristic patterns that have been found of strongly increasing concentrations and increasing fluxes or moderately increasing concentrations and decreasing fluxes with colder climate can be obtained solely by a general change (i.e., the same change for all impurities) in the ratio between transit time and residence time. The stronger increase of the concentration in the ice is obtained by using a larger t^*/τ^* value. On the other hand, decreasing concentrations and fluxes with a colder climate imply a decrease in the airborne concentration at the

Tellus B/46/5-6

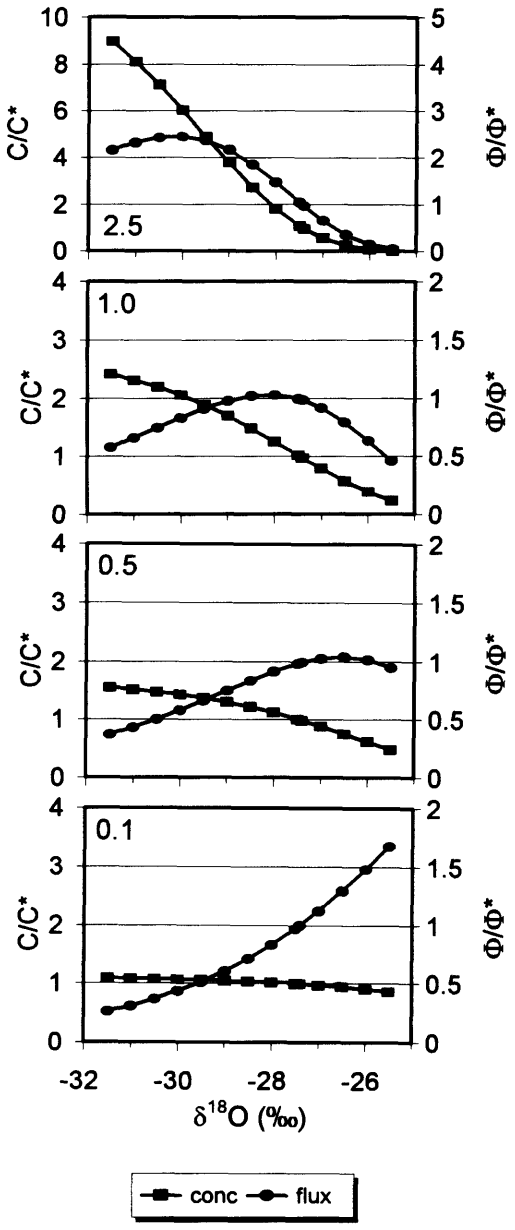

Fig. 13. Model results of the relative concentration in the ice (C_{ice}/C^*_{ice}) and the relative wet deposition flux (Φ_{wet}/Φ^*_{wet}) at Renland, plotted against $\delta^{18}O$, for four different t^*/τ^* ratios (2.5, 1.0, 0.5 and 0.1, respectively) with the same gradual change of the ratio n/k to 0.1 in stage 2. The late Holocene is the reference state. The airborne concentration at the source and the local scavenging ratio at Renland are kept constant (i.e., $C(0)_{air}/C(0)^*_{air} = 1$ and $W/W^* = 1$).

source, a decrease in the local scavenging ratio or a change of source location (the source area has to be located so much further away that the transit time increases more than the residence time, i.e., the ratio n/k has to be above 1).

6.4.5. Estimation of t^* and τ^*. Important for the result of the model simulation is the choice of reference ratio t^*/τ^* and not the individual numbers for t^* and τ^*. Guidelines for reference residence times (τ^*) can be taken from a model of the residence time of aerosol particles as a function of particle radius (r) under present climatic conditions (Jaenicke, 1988). An interval of residence times from 28 days for $r = 0.1$–0.7 μm to 10 days for $r = 2$ μm is presented. These residence times are valid for an aerosol scale height above the boundary layer ($H > 1.5$ km) where wet deposition is the only removal process. The Greenland ice sheet receive precipitation representative of altitudes above 2.5–4.5 km. Shorter residence times are expected if the lower troposphere and the boundary layer are considered (i.e., close to the source). Slinn (1983) has suggested an average residence time for sulphate (fine mode particles) on the order of one week and shorter residence times for coarse mode particles. Langner and Rodhe (1991) have suggested an average residence time for sulphate of 4.6 to 5.2 days. Some impurities are transported as gases, at least initially, which further complicates the estimate of reference residence times.

The reference transit time (t^*) is quite difficult to estimate since the locations of the major influencing source areas are not very well known even for present conditions. The most likely range of t^*/τ^* is found to be between 0 and 2.5 (Fig. 12). This gives a large span of possible values of t^* (from 1 day to a maximum of 70 days for fine mode particles and 25 days for coarse mode particles).

6.4.6. Application. Cl^-, Na^+, nss SO_4^{2-} and the biogenic fraction of nss K^+ are probably found in a smaller size fraction than the crustally derived nss Ca^{2+}, nss Mg^{2+} and dust. If the transit times are similar for all these impurities, shorter residence times for the larger crustally derived impurities will give higher t^*/τ^* values. The patterns of changes in concentrations and fluxes (Fig. 11) for the crustally derived impurities can be reproduced with t^*/τ^* values in the range 1–2.5 and a general decrease in the ratio n/k (i.e., any value of n/k in the likely range is chosen and kept for all impurities). No increase in airborne concen-

trations at the sources or change of the local scavenging ratios are necessary, however possible, to explain the strongly enhanced concentrations found during the glacial period. Dry deposition of these impurities at Renland will further enhance the concentration in the ice ($C_{ice}/C^*_{ice} > C(0)_{air}/C(0)^*_{air}$) and the total flux ($\Phi_{tot}/\Phi^*_{tot} > \Phi_{wet}/\Phi^*_{wet}$).

The patterns of changes for Cl^-, Na^+, nss SO_4^{2-} (Fig. 11) are consistent with t^*/τ^* values below 0.75 and the same general decrease in the ratio n/k as chosen for the crustally derived impurities. The concentration of nss SO_4^{2-} increases faster in the cold glacial stages ($\delta^{18}O < -30‰$) which can indicate an addition of a new source of nss SO_4^{2-}, e.g., crustally derived $CaSO_4$. This nss SO_4^{2-} will then be in the coarse mode and dry deposition becomes important. The dry deposition process itself will increase the concentration in the ice therefore only a small addition is necessary. Another possibility is that the nss SO_4^{2-} arrives attached to the crustally derived aerosol due to a neutralising process in the atmosphere with alkaline droplets, as has been suggested for the SH aerosol (Legrand et al., 1988). The nss SO_4^{2-} would then be affected by the dry deposition process of the crustal aerosol. If this neutralising process takes place in the atmosphere, no additional sources of nss SO_4^{2-} or inrease in strength of already existing sources are necessary to give the measured concentrations and fluxes.

The patterns of the last group, containing $CH_3SO_3^-$, NO_3^- and NH_4^+, with decreasing concentrations with colder climate can only be reproduced with decreasing airborne concentrations at the sources or decreasing local scavenging ratios if they are affected by a general decrease in the ratio n/k. However, the chemical transformations in the atmosphere of the nitrogen compounds are so complex that residence times and transit times and their change with climate are highly uncertain. In the case of $CH_3SO_3^-$, it is interesting to note the divergence from the patterns of nss SO_4^{2-}, which can be interpreted as (1) the majority of nss SO_4^{2-} is not originating from the same source as $CH_3SO_3^-$ (whose source strength decreases or the source area is moved further away), (2) the initial branching ratio during the DMS oxidation is altered due to the climate change (or due to a change in influencing source area) which can be seen as an increase in the source strength of nss SO_4^{2-} and a decrease in the source strength of $CH_3SO_3^-$, or (3) the scavenging ratios for nss SO_4^{2-} and $CH_3SO_3^-$, respectively, are not influenced by the climate change in a similar way which will cause a fractionation between these two ions along the transport path. However, the linear relationship between the ratio R and $\delta^{18}O$ (Fig. 9) is surprising if different sources are responsible for the concentration changes of nss SO_4^{2-} and $CH_3SO_3^-$. To support the second hypothesis, a better understanding of the processes determining initial branching ratios in different areas is needed. The third hypothesis implies that the scavenging ratio decreases for $CH_3SO_3^-$ with a colder climate. If due to a decreasing amount of riming, nss SO_4^{2-} would also be affected in the same direction. Other conditions that alter the scavenging ratios have to be considered, such as changed size distributions of the pre-existing aerosol or a different chemistry due to the dominance of an alkaline aerosol, but then the explanation of the linear relationship to temperature has to be found for these conditions.

6.5. Interpretation of influence on the composition of the atmosphere

The simple model simulation described above shows that for many of the impurities present in the ice, the changes in the physical conditions of the atmosphere are sufficient in themselves to account for all the observed changes in the concentrations. Further, it shows that interpretations of changes in source emissions have to be made with caution from records of deposition. It also shows how important it is to understand the reasons behind the observed changes in impurity concentrations in ice cores before extrapolating the results to a global scale. The different possible explanations for the variations seen in glacial records will have different implications for the total burden of impurities in the global atmosphere. If an increased source strength is responsible for enhanced concentrations in the ice sheets, the airborne concentrations of that impurity would be proportionally higher everywhere along the transport path. If enhanced concentrations in the ice are due to changes in residence times and transit times, the glacial scenario presented above will mean a more evenly distribution of all impurities with decreased airborne concentrations close to the sources but increased airborne concentrations far away (e.g., at the poles). The total burden of impurities in the

atmosphere will be enhanced in both cases but the enhancement can be significantly different as is shown in the following.

Integration of eq. (2) over the transport path will give the total content, M (M), of an impurity in the atmosphere. The total content, relative to the late Holocene conditions, can thus be described by:

$$M/M^* \propto C(0)_{air}/C(0)^*_{air}k/n. \quad (10)$$

As a consequence, the total content of nss SO_4^{2-} in the atmosphere is increased by a factor of ten if the observed two-fold increase of the nss SO_4^{2-} concentration in the ice at Renland is due to a change of the residence time and transit time corresponding to $n/k = 0.1$, but only increased by a factor of two if the same observed two-fold increase is due to a two-fold increase in source strength. In the case of nss Ca^{2+}, the two possibilities of a ten-fold increase in source strength or the estimated maximal change of the residence time and transit time (i.e., $n/k = 0.1$) will both give a ten times higher load of nss Ca^{2+} in the atmosphere.

Thus, the effect of changes in the physical conditions of the atmosphere can be more important for the composition of the atmosphere than changes in source emissions. Changes in the hydrological cycle and the general circulation can have a large impact on the radiative properties of the atmosphere. A climate forcing mechanism may be found in the dynamics of the atmosphere. This shows that it is essential to attain a better knowledge of the atmospheric conditions during glacial stages to take the full advantage of the ice core records.

6.6. *Comparison with Southern Hemisphere records*

When comparing Greenland data with the results from studies performed on ice cores from Antarctica in the SH, many similarities are found but also some striking differences. The only data set for a full comparison with the Renland data, both in terms of time span and number of impurities, is extracted from the Vostok ice core from the East Antarctic plateau (Legrand et al., 1988; Legrand et al., 1991). The variations in the stable isotope records are very similar (Johnsen et al., 1992a) which suggests a roughly parallel climatic development in the two hemispheres. Further, the variations in the impurity profiles are clearly coupled to the climate changes. Comparing absolute concentrations may be misleading due to a factor of 20 difference in accumulation rate and thus a higher influence of dry deposition at Vostok. Also the wet deposition mechanisms may be different due to large temperature differences between Greenland and Antarctica. However, the absolute concentrations in the Holocene are of the same order of magnitude (usually closer) and the largest differences can be explained by the different surroundings (i.e., oceans in the SH and continents in the NH). The concentrations of sea salt and crustally derived impurities increase with colder climate in both ice cores. The sea salt concentration is more strongly enhanced at Vostok than at Renland during cold stages. The Cl^-/Na^+ ratio is also varying considerable more at Vostok, suggesting a fractionation of the sea salt which is not indicated by the Renland data. The sea salt is an important constituent of the total impurity content at Vostok while minor at Renland. During the coldest stages, the Renland ionic budget is totally dominated by crustally derived ions. The Renland ice (as the rest of the Greenland ice sheet) is alkaline during these stages, indicating a large input of mainly $CaCO_3$, in contrast to ice from Antarctica which is slightly acidic overall. The importance of nss Ca^{2+} in the ionic budget is low at Vostok but its relative increase with colder climate is even higher than at Renland. Also the dust flux is more strongly increased (by a factor of 15 in stage 2 compared to Holocene) at Vostok (Petit et al., 1990) than at Renland. The concentration of nss SO_4^{2-} is enhanced in cold stages in both ice cores, but at Renland stronger correlated to the crustally derived impurities. The importance of nss SO_4^{2-} in the ionic budget is lower at Renland than at Vostok in all stages.

The most striking differences are found in the records of NO_3^-, NH_4^+ and $CH_3SO_3^-$. The concentrations of these ions decrease with colder climate at Renland while increase at Vostok. However, the importance of NO_3^- and NH_4^+ in the ionic budget is higher at Renland than at Vostok. The NO_3^- variation at Vostok is correlated to the crustally derived impurities while no such correlation is found at Renland. The decrease of $CH_3SO_3^-$ at Renland with colder climate leads to a decrease in the molar ratio R ($CH_3SO_3^-$/nss SO_4^{2-}) while R increases with colder climate at Vostok. Linear relationships

between R and isotopic temperature are found both at Vostok (Legrand et al., 1992b) and at Renland but with opposite signs. This is discussed further in Hansson and Saltzman (1993).

If applying the model to the SH records, the differences in deposition mechanisms between NH and SH have to be taken into account. When dry deposition is the dominant mechanism, a decrease in accumulation rate will increase the concentration in the ice but the flux will be independent of the accumulation rate. The relative changes of impurity concentrations in the ice are generally larger at Vostok than Renland, and increasing with colder climate for all impurities, in accordance with a dominance of the dry deposition mechanism. In addition, a general conclusion from the model simulation is that the further away the sources, the more important are changes in the residence times. Vostok is far away from all terrestrial and marine sources and all changes of the residence times will have a large effect on the impurity concentrations at Vostok. The effect of a longer residence time may possibly outrival the effect of a decrease in airborne concentration at the source which might explain the different records of biogenic impurities at Vostok and Renland.

7. Conclusions

This work represents the first comprehensive study of both anions, cations and insoluble impurities deposited on Greenland during interglacial and glacial conditions. Similar studies have previously been presented only for the SH. Continuous profiles with high resolution are extracted between 10 and 120 ka B.P. and from the 19th century. The high resolution reveals fast and large variations in the concentration profiles of crustally derived impurities (dust, nss Ca^{2+}, nss Mg^{2+} and nss K^+) and nss SO_4^{2-}, anti-correlated to the fast variations in the climatic record ($\delta^{18}O$) which means that high concentrations are associated with low temperatures. The variations of the sea salt components (mainly Na^+ and Cl^-) are also anti-correlated to $\delta^{18}O$ but with a smaller amplitude. No fractionation between the sea salt elements is indicated but possibly a crustal contribution to the Na^+ concentration during the coldest glacial stages. Impurities with a strong biogenic contribution (NO_3^-, NH_4^+ and $CH_3SO_3^-$) correlate with the long term trend of $\delta^{18}O$ as opposed to the anti-correlation found in the SH ice cores. Thus, low concentrations of these impurities are found in the cold glacial stages in the Renland ice core. However, these impurities also sometimes show an anti-correlation on the time scale of hundreds of years. Physical changes in the atmosphere which influence all impurities in a similar way are most probably determinant for the similar fine structure in all profiles.

A simple model is formulated to reveal the influence on the concentration profiles of physical changes in the atmosphere compared to climate induced changes in source emissions (e.g., determined by sea level changes, changes in the vegetation cover on the continents or biogenic activity in the oceans). The change of two parameters, concentration in the ice and wet deposition flux, with climate are examined. The measured changes in concentrations in the ice and total deposition fluxes for the different impurities can be divided into three groups; (1) increasing concentrations and fluxes with colder climate (dust, nss Ca^{2+} and nss Mg^{2+}), (2) increasing concentrations but decreasing fluxes (Na^+, Cl^-, nss SO_4^{2-} and nss K^+), and (3) decreasing concentrations and fluxes (NO_3^-, NH_4^+ and $CH_3SO_3^-$). The patterns of the first two groups can be explained entirely by a general change in residence times and transit times due to decreased precipitation rates along the transport paths and a stronger general circulation in colder climatic stages. No increase in source emissions is necessary, however possible, to explain also the ten-fold increased impurity concentrations in the Renland ice core in cold glacial stages. With the same general change in residence times and transit times affecting the third group, specific changes (e.g., decreased source emissions with colder climate) are necessary to explain the patterns of this group. The total content of impurities in the atmosphere will be higher if physical changes in the atmosphere rather than source emission changes are responsible for the observed variations in the Renland ice core. Thus, physical changes in the atmosphere may have a large impact on the radiative properties of the atmosphere. This suggests that a climate forcing mechanism may be found in the dynamics of the atmosphere.

The model simulation only deals with mean values in the different climatic stages and estimated mean changes of the various influencing param-

eters. More information may be obtained from the Renland record by taking advantage of the continuity and the high resolution, but it requires a better understanding of the hydrological cycle and the general circulation of the atmosphere during glacial conditions. Comparable data with high resolution from other locations are also required to go further in the interpretation of environmental changes from ice core records.

8. Acknowledgements

I would like to thank all participants in the Nordic Renland Project for excellent co-operation during the field campaigns and the colleagues at the Niels Bohr Institute, Department of Geophysics, University of Copenhagen, for all support during the analytical part of this work. I am grateful to Eric Saltzman for providing the facilities for the methanesulphonate analysis at the Rosenstiel School of Marine and Atmospheric Science, University of Miami. Kim Holmén, Henning Rodhe and Hans-Christen Hansson are acknowledged for valuable comments on the manuscript. Robert Mulvaney is acknowledged for a careful review of the final manuscript. Swedish Natural Science Research Council and Nordic Council of Ministers are acknowledged for financial support.

REFERENCES

Alley, R. B., Meese, D. A., Shuman, C. A., Gow, A. J., Taylor, K. C., Grootes, P. M., White, J. W. C., Ram, M., Waddington, E. D., Mayewski, P. A. and Zielinski, G. A. 1993. Abrupt increase in Greenland snow accumulation at the end of the Younger Dryas event. *Nature* **362**, 527–529.

Ayers, G. P., Ivey, J. P. and Gillett, R. W. 1991. Coherence between seasonal cycles of dimethyl sulphide, methanesulphonate and sulphate in marine air. *Nature* **349**, 404–406.

Barrie, L. A. 1985a. Scavenging ratios, wet deposition and in-cloud oxidation: an application to oxides of sulphur and nitrogen. *J. Geophys. Res.* **90 (D3)**, 5789–5799.

Barrie, L. A. 1985b. Atmospheric particles. Their physical and chemical characteristics, and deposition processes relevant to the chemical composition of glaciers. *Annals of Glaciology* **7**, 100–108.

Bates, T. S., Calhoun, J. A. and Quinn, P. K. 1992a. Variations in the methanesulfonate to sulfate molar ratio in submicrometer marine aerosol particles over the South Pacific Ocean. *J. Geophys. Res.* **97**, 9859–9865.

Bates, T. S., Lamb, B. K., Guenther, A., Dignon, J. and Stoiber, R. E. 1992b. Sulfur emissions to the atmosphere from natural sources. *J. Atmos. Chem.* **14**, 315–337.

Beer, J., Siegenthaler, U., Bonani, G., Finkel, R. C., Oeschger, H., Suter, M. and Wölfli, W. 1988. Information on past solar activity and geomagnetism from ^{10}Be in the Camp Century ice core. *Nature* **331**, 675–679.

Berresheim, H. 1987. Biogenic sulfur emissions from the subantarctic and antarctic oceans. *J. Geophys. Res.* **92**, 13245–13262.

Calvert, J. G., Su, F., Bottenheim, J. W. and Strausz, O. P. 1978. Mechanism of the homogeneous oxidation of sulfur dioxide in the troposphere. *Atmos. Environ.* **12**, 197–226.

Clausen, H. B. and Hammer, C. U. 1988. The Laki and Tambora eruptions as revealed in Greenland ice cores from 11 locations. *Annals of Glaciology* **10**, 16–22.

Clausen, H. B. and Langway, C. C. Jr. 1989. The ionic deposits in polar ice cores. In: *The environmental record in glaciers and ice sheets* (eds. H. Oeschger and C. C. Langway, Jr.). John Wiley & Sons Limited, 225–247.

COHMAP members. 1988. Climatic changes of the last 18,000 years: Observations and model simulations. *Science* **241**, 1043–1052.

Cragin, J. H., Herron, M. M., Langway, C. C. Jr. and Klouda, G. 1977. Interhemispheric comparison of changes in the composition of atmospheric precipitation during the late Cenozoic era. In: *Polar oceans* (ed. M. J. Dunbar). Proceedings of the Polar Oceans Conference, McGill Univ., Montreal, May 1974, Calgary, Alberta, Arctic Institute of North America, 617–631.

Dansgaard, W., Johnsen, S. J., Clausen, H. B. and Gundestrup, N. 1973. Stable isotope glaciology. *Meddr. Grönland Geosci.* **197**, 1–53.

Dansgaard, W., Clausen, H. B., Gundestrup, N., Hammer, C. U., Johnsen, S. J., Kristinsdottir, P. M. and Reeh, N. 1982. A new Greenland deep ice core. *Science* **218**, 1273–1277.

Dansgaard, W., Johnsen, S. J., Clausen, H. B., Dahl-Jensen, D., Gundestrup, N., Hammer, C. U. and Oeschger, H. 1984. North Atlantic Climatic oscillations revealed by deep Greenland Ice Cores. In: *Climatic processes and climate sensitivity* (eds. J. E. Hansen and T. Tagahashi). Geophysical Monograph 29, Maurice Ewing Volume 5, 288–298.

Dansgaard, W., Johnsen, S. J., Clausen, H. B., Dahl-Jensen, D., Gundestrup, N. S., Hammer, C. U.,

Hvidberg, C. S., Steffensen, J. P., Sveinbjörnsdottir, A. E., Jouzel, J. and Bond, G. 1993. Evidence for general instability of past climate from a 250-kyr ice-core record. *Nature* **364**, 218–220.

Davidson, C. I., Jaffrezo, J.-L., Mosher, B. W., Dibb, J. E., Borys, R. D., Bodhaine, B. A., Rasmussen, R. A., Boutron, C. F., Gorlach, U., Cachier, H., Ducret, J., Colin, J.-L., Heidam, N. Z., Kemp, K. and Hillamo, R. 1993. Chemical constituents in the air and snow at Dye 3, Greenland: 1. Seasonal variations. *Atmos. Environ.* **27A**, 2709–2722.

Delmas, R. J. 1993. A natural artefact in Greenland ice-core CO_2 measurements. *Tellus* **45B**, 391–396.

Finkel, R. C. and Langway, C. C. Jr. 1985. Global and local influences on the chemical composition of snow-fall at Dye 3, Greenland: The record between 10 and 40 ka B.P. and 40 ka B.P. *Earth and Planetary Science Letters* **73**, 196–206.

Fuhrer, K., Neftel, A., Anklin, M. and Maggi, V. 1993. Continuous measurements of hydrogen peroxide, formaldehyde, calcium and ammonium concentrations along the new GRIP ice core from the Summit, Central Greenland. *Atmos. Environ.* **27A**, No. 12, 1873–1880.

Greenland Ice-core Project (GRIP) Members. 1993. Climate instability during the last interglacial period recorded in the GRIP ice core. *Nature* **364**, 203–207.

Grootes, P. M., Stuiver, M., White, J. W. C., Johnsen, S. and Jouzel, J. 1993. Comparison of oxygen isotope records from the GISP2 and GRIP Greenland ice cores. *Nature* **366**, 552–554.

Hammer, C. U. 1977. Dust studies on Greenland ice cores. Proceedings of Symposium on Isotopes and Impurities in Snow and Ice, International Association of Hydrological Science, Commision of Snow and Ice, International Union on Geophysics and Geodesy, XVI General Assembly, Grenoble Aug. Sept., 1975. *IAHS-AISH publication* **118**, 365–370.

Hammer, C. U. 1980. Acidity of polar ice cores in relation to absolute dating, past volcanism, and radio-echoes. *J. Glaciology* **25**, 359–372.

Hammer, C. U. 1983. Initial direct current in the buildup of space charges and acidity of ice cores. *J. Phys. Chem.* **87**, 4099–4103.

Hammer, C. U., Clausen, H. B., Dansgaard, W., Neftel, A., Kristinsdotter, P. and Johnson, E. 1985. Continuous impurity analysis along the Dye 3 deep core. In: *Greenland ice core: geophysics, geochemistry, and the environment.* Geophys. Monogr. 33 (eds. C. C. Langway, Jr., H. Oeschger, and W. Dansgaard), AGU, Washington DC, 90–94.

Hansen, B. L. and Langway, C. C. Jr. 1966. Deep core drilling in ice and core analyses at Camp Century, Greenland, 1961–66. *United States Antarctic Journal* **1**, 207–208.

Hansson, M. E. and Saltzman, E. S. 1993. The first Greenland ice core record of methanesulfonate and sulfate over a full glacial cycle. *Geophys. Res. Lett.* **20**, 1163–1166.

Hegg, D. A. 1990. Heterogeneous production of cloud condensation nuclei in the marine atmosphere. *Geophys. Res. Lett.* **17**, 2165–2168.

Herron, M. M. and Langway, C. C. Jr. 1985. Chloride, nitrate, and sulfate in the Dye 3 and Camp Century, Greenland ice cores. In: *Greenland ice core: geophysics, geochemistry, and the environment.* Geophys. Monogr. 33 (eds. C. C. Langway, Jr., H. Oeschger, and W. Dansgaard), AGU, Washington DC, 77–84.

Hynes, A. J., Wine, P. H. and Semmes, D. H. 1986. Kinetics and mechanism of OH reactions with organic sulfides. *J. Phys. Chem.* **90**, 4148–4156.

Jaenicke, R. 1988. Aerosol physics and chemistry. In Landolt-Börnstein: *Numerical data and functional relationships in science and technology.* New Series, Group V: Geophysics and space research, vol. 4: Meteorology (ed. G. Fischer). Subvolume (b) Physical and chemical properties of the air. Springer, Berlin, pp. 391–457.

Johnsen, S. J., Dansgaard, W., Clausen, H. B. and Langway, C. C. Jr. 1972. Oxygen isotope profiles through the Antarctic and Greenland ice sheets. *Nature* **235**, 429–434.

Johnsen, S. J., Dansgaard, W., Gundestrup, N., Hansen, S. B., Nielsen, J. O. and Reeh, N. 1980. A fast light-weight core drill. *J. Glaciology* **25**, 169–174.

Johnsen, S. J., Dansgaard, W. and White, J. W. C. 1989. The origin of Artic precipitation under present and glacial conditions. *Tellus* **41B**, 452–468.

Johnsen, S. J., Clausen, H. B., Dansgaard, W., Gundestrup, N., Hansson, M., Jonsson, P., Steffensen, J. P. and Sveinbjörnsdottir, A. E. 1992a. A "deep" ice core from East Greenland. *Meddr. Grönland Geosci.* **30**, 22 pp.

Johnsen, S. J., Clausen, H. B., Dansgaard, W., Fuhrer, K., Gundestrup, N., Hammer, C. U., Iversen, P., Jouzel, J., Stauffer, B. and Steffensen, J. P. 1992b. Irregular glacial interstadials recorded in a new Greenland ice core. *Nature* **359**, 311–313.

Johnsen, S. J. and Dansgaard, W. 1992. On flow model dating of stable isotope records from Greenland ice cores. In: *The last deglaciation, absolute and radiocarbon chronologies* (ed. E. Bard). Proceedings of NATO workshop, Erice, Italy, Dec. 1990, NATO Advanced Studies Institute Series, Vol. I 2., 13–24.

Joussaume, S. 1993. Paleoclimatic tracers: An investigation using an atmospheric general circulation model under ice age conditions. 1. Desert dust. *J. Geophys. Res.* **98 (D2)**, 2767–2805.

Langner, J. 1991. *Sulfur in the troposphere: a global three-dimensional model study.* PhD Thesis. Dept. of Meteorology, Stockholm University.

Langner, J. and Rodhe, H. 1991. A global three-dimensional model of the tropospheric sulfur cycle. *J. Atmos. Chem.* **13**, 225–263.

Langway, C. C. Jr., Clausen, H. B. and Hammer, C. U. 1988. An inter-hemispheric volcanic time-marker in ice cores from Greenland and Antarctica. *Annals of Glaciology* **10**, 102–108.

Legrand, M. 1987. Chemistry of Antarctic snow and ice. *J. de Phys.* **48**, 77–86.

Legrand, M. and Delmas, R. J. 1987a. Environmental changes during last deglaciation inferred from chemical analysis of the Dome C ice core. In: *Abrupt climatic change* (eds. W. H. Berger and L. D. Labeyrie), Reidel, 247–259.

Legrand, M. R. and Delmas, R. J. 1987b. Experimental protocol for the chemical analysis of snow, firn and ice cores. In: *Seasonal snowcovers: physics, chemistry, hydrology* (eds. H. G. Jones and W. J. Orville-Thomas), Reidel, 225–254.

Legrand, M. R., Lorius, C., Barkov, N. I. and Petrov, V. N. 1988. Vostok (Antarctica) ice core: Atmospheric chemistry changes over the last climatic cycle (160,000 years). *Atmos. Environ.* **22**, 317–331.

Legrand, M., Feniet-Saigne, C., Saltzman, E. S., Germain, C., Barkov, N. I. and Petrov, V. N. 1991. Ice-core record of oceanic emissions of dimethylsulphide during the last climatic cycle. *Nature* **350**, 144–146.

Legrand, M., De Angelis, M., Staffelbach, T., Neftel, A. and Stauffer, B. 1992a. Large perturbations of ammonium and organic acids content in the Summit-Greenland ice core. Fingerprint from forest fires? *Geophys. Res. Lett.* **19**, 473–475.

Legrand, M., Feniet-Saigne, C., Saltzman, E. S. and Germain, C. 1992b. Spatial and temporal variations of methanesulfonic acid and non sea salt sulfate in antarctic ice. *J. Atmos. Chem.* **14**, 245–260.

Mayewski, P. A., Spencer, M. J. and Lyons, W. B. A review of Glaciochemistry with particular emphasis on the recent record of sulfate and nitrate. 1992. In: *Trace gases and the biosphere* (eds. B. Moore III and D. Schimel), UCAR, Office for interdisciplinary Earth Studies, Boulder, Colorado, 177–199.

Mayewski, P. A., Meeker, L. D., Whitlow, S., Twickler, M. S., Morrison, M. C., Alley, R. B., Bloomfield, P. and Taylor, K. 1993. The Atmosphere During the Younger Dryas. *Science* **261**, 195–197.

Palais, J. M. and Legrand, M. 1985. Soluble impurities in the Byrd Station ice core, Antarctica: Their origin and sources. *J. Geophys. Res.* **90 (C1)**, 1143–1154.

Penkett, S. A., Jones, B. M. R., Brice, K. A. and Eggleton, A. E. J. 1979. The importance of atmospheric ozone and hydrogen peroxide in oxidising sulphur dioxide in cloud and rain water. *Atmos. Environ.* **13**, 123–137.

Petit, J. R., Mounier, L., Jouzel, J., Korotkevich, Y. S., Kotlyakov, V. I. and Lorius, C. 1990. Palaeoclimatological and chronological implications of the Vostok core dust record. *Nature* **343**, 56–58.

Quinn, P. K., Charlson, R. J. and Bates, T. S. 1988. Simultaneous observations of ammonia in the atmosphere and ocean. *Nature* **335**, 336–338.

Scott, B. C. 1981. Sulfate wash out ratios in winter storms. *Journal of Applied Meteorology* **20**, 619–625.

Slinn, W. G. N. 1983. Air-to-sea transfer of particles. In: *Air-sea exchange of gases and particles* (eds. P. S. Liss and W. G. N. Slinn). NATO ASI Series C108, Reidel, Dordrecht, 299–405.

Slinn, W. G. N. 1984. Precipitation scavenging. In: *Atmospheric science and power production* (ed. D. Randerson). Technical Information Center, Oak Ridge, TN, US Department of Energy.

Spiro, P. A., Jacob, D. J. and Logan, J. A. 1992. Global inventory of sulfur emissions with $1° \times 1°$ resolution. *J. Geophys. Res.* **97**, 6023–6036.

Staffelbach, T., Stauffer, B. and Oeschger, H. 1988. A detailed analysis of the rapid changes in ice-core parameters during the last ice age. *Annals of Glaciology* **10**, 167–170.

Stoiber, R. E., Williams, S. N. and Huebert, B. 1987. Annual contribution of sulfur dioxide to the atmosphere by volcanoes. *J. Volcanol. Geotherm. Res.* **33**, 1–8.